

Geochemical constraints on the geodynamic setting of Alborz-Azerbaijan Cenozoic magmatism

Maryam Honarmand^{a,*}, Annique van der Boon^{b,c}, Franz Neubauer^d, Bianca Heberer^d, Qiuli Li^e, Klaudia F. Kuiper^f, Paul R.D. Mason^b, Wout Krijgsman^b

^a Department of Earth Sciences, Institute for Advanced Studies in Basic Sciences (IASBS), P.O. Box 45195-1159, Zanjan, Iran

^b Department of Earth Sciences, Utrecht University, The Netherlands, Princetonlaan 8a, 3584 CB Utrecht, the Netherlands

^c Now at: Centre for Planetary Habitability (PHAB), University of Oslo, ZEB-building, Sem Sælands vei 2 A, 0371 Oslo, Norway

^d Department of Environment and Biodiversity, University of Salzburg, A-5020 Salzburg, Austria

^e State Key Laboratory of Lithospheric Evolution, Institute of Geology and Geophysics, Chinese Academy of Sciences, Beijing 100029, China

^f Dept. of Earth Sciences, Faculty of Science, Vrije Universiteit Amsterdam, De Boelelaan 1085, 1081 HV Amsterdam, the Netherlands

ARTICLE INFO

Editor: Dr. Balz Kamber

Keywords:

Neotethyan subduction

Eocene

K-rich magmatism

Slab tear

Alborz

Iran

ABSTRACT

The Alborz Mountains in northern Iran form part of the Tethyan orogenic belt and surround the South Caspian Basin. The geology of the western Alborz Mountains is dominated by Eocene mafic to intermediate high-K calc-alkaline-alkaline shoshonitic and minor Oligo-Miocene magmatic rocks, displaying arc geochemical characteristics (e.g., negative Nb, Ta, Ti anomalies). Cenozoic magmatism across this region in western Asia has been explained by a diversity of contrasting geodynamic models involving (multiple slab) subduction and slab-breakoff. The aim of this study is to better constrain the geodynamic setting of magmatism during regional convergence through the investigation of the relatively unstudied Alborz-Azerbaijan magmatic belt. Incompatible trace element geochemistry of Eocene lavas from this belt is distinctive and indicates that they were generated by relatively low-degrees of partial melting of the subcontinental lithospheric mantle with a contribution of asthenosphere melts. Miocene lavas from the Alborz and northern Urmia–Dokhtar magmatic arc (UDMA) share a common arc geochemical signature. Zircon $\epsilon\text{Hf}(t)$ values of the Miocene magmatic rocks from the Alborz and northern UDMA range from -0.4 to 11.7 , suggesting incorporation of older continental crust mixed with a more juvenile component. New thermochronological data (fission track and (U-Th)/He on apatite) from the late Eocene plutonic bodies in the Tarom area track exhumational cooling at moderate rates following rapid post-emplacement magmatic cooling at ca. 40 Ma. The geochemical data in conjunction with geological and published geophysical results imply a bending or disruption in the subducting slab under the Tarom area, associated with slab roll-back during the Eocene. This process led to the arc-front displacement and a greater contribution of deep enriched mantle in the Alborz magmas compared to those from the high-flux magmatic event along the Alborz and Urmia–Dokhtar magmatic arc (UDMA), triggered by asthenospheric upwelling and mixing with melts derived from earlier metasomatized subcontinental lithospheric mantle.

1. Introduction

The Alpine-Himalayan orogenic belt, which stretches from Europe towards East Asia, forms a continuous mountain chain that was deformed and exhumed during the Mesozoic and Cenozoic, due to closure of the Neotethys Ocean. The Neotethys Ocean initially formed in the late Carboniferous to early Permian after Cimmerian continental

fragments (represented by rocks in modern Iran, Turkey, central Afghanistan and south Tibet, e.g., Stampfli, 2000) broke away from the north-eastern margin of Gondwana. During the late Triassic to Jurassic, these microcontinents migrated northwards and sutured with Eurasia, closing the Paleotethys Ocean. Subsequent northward migration of Africa, Arabia, and India resulted in subduction of the Neotethys Ocean beneath the Cimmerian fragments that had previously merged with

* Corresponding author.

E-mail addresses: m.honarmand@iasbs.ac.ir (M. Honarmand), a.van.der.boon@geo.uio.no (A. van der Boon), Franz.Neubauer@plus.ac.at (F. Neubauer), bianca.heberer@plus.ac.at (B. Heberer), liqiuli@mail.iggcas.ac.cn (Q. Li), K.F.Kuiper@vu.nl (K.F. Kuiper), p.mason@uu.nl (P.R.D. Mason), W.Krijgsman@uu.nl (W. Krijgsman).

<https://doi.org/10.1016/j.chemgeo.2023.121889>

Received 28 June 2022; Received in revised form 9 December 2023; Accepted 12 December 2023

Available online 16 December 2023

0009-2541/© 2023 Elsevier B.V. All rights reserved.

Eurasia, leading to voluminous magmatism.

Northward subduction of the Neotethys slab was initiated in the Triassic to Early Jurassic (Berberian and King, 1981; Stampfli and Borel, 2002; Agard et al., 2011; Hassanzadeh and Wernicke, 2016; Chiu et al., 2017), peaking at ca. 170 Ma (Hassanzadeh and Wernicke, 2016), and continued further into the Cenozoic. In contrast, the main peak of magmatism was in the Eocene and Miocene. The subduction of the Neotethys oceanic lithosphere beneath Eurasia occurred not as a single uniform event, but has been related to multiple tectonic processes such as the formation of multiple magmatic arcs, retreating subduction, back-arc extension (e.g., Rosenbaum et al., 2002), slab break off (e.g., Agard et al., 2011) and oblique subduction (e.g., Mohajjel et al., 2003; Sarkarinejad and Azizi, 2008; Mouthereau et al., 2012). Neotethys closure culminated in continental collision between Arabia and Eurasia, which led to formation of the Zagros Mountains on the Arabian plate and uplift of the Iranian plateau on the Eurasian plate. Timing of this continental collision, however, is controversial, with estimates ranging from the late Cretaceous to Miocene times (ca. 5 Ma) (see review in McQuarrie and van Hinsbergen, 2013).

The Zagros Mountains extend towards the northwest near the Turkish–Iranian border and to the southeast in the Makran region, where subduction is still active (e.g., Regard et al., 2010; Smit et al., 2010;

Fig. 1a). The Mesozoic NW-trending Sanandaj–Sirjan and the Cenozoic NW-trending Urmia–Dokhtar magmatic arcs trend sub-parallel to the Main Zagros fold-and-thrust belt (Fig. 1a) and have been the subject of numerous structural, geochemical and isotopic studies (e.g., Omrani et al., 2008; Ghasemi and Talbot, 2006; Agard et al., 2011; Verdel et al., 2011; Mohajjel et al., 2003; Esna-Ashari et al., 2012; Azizi and Jahangiri, 2008; Mahmoudi et al., 2011; Honarmand et al., 2013, 2014; Chiu et al., 2013; Yeganehfar et al., 2013; Sepahi and Malvandi, 2008; Maghdour-Mashhour et al., 2021). Compared to the relatively well-studied UDMA and the Sanandaj–Sirjan zone (SSZ), much less is known about the Alborz–Azerbaijan belt, which stretches from the Azerbaijan Province into the Alborz Mountains. The Alborz–Azerbaijan belt is distinguished from the UDMA by the presence of more potassic magmatism, particularly of Eocene (56–34 Ma) age, the time of a coeval magmatic flare-up in both the UDMA and Alborz. Overall, the geodynamic setting of Eocene magmatism along the Alborz belt is considered as back-arc/rear-arc (e.g., Vincent et al., 2005; Verdel et al., 2011; Agard et al., 2011; Asiabanha and Foden, 2012; Nabatian et al., 2016a; Moghadam et al., 2020), continental arc (Asiabanha et al., 2009) or post-collisional (e.g., Aghazadeh et al., 2011; Castro et al., 2013).

In this study, we present new geochemical data to determine the petrogenetic evolution of Cenozoic magmatic rocks in the western

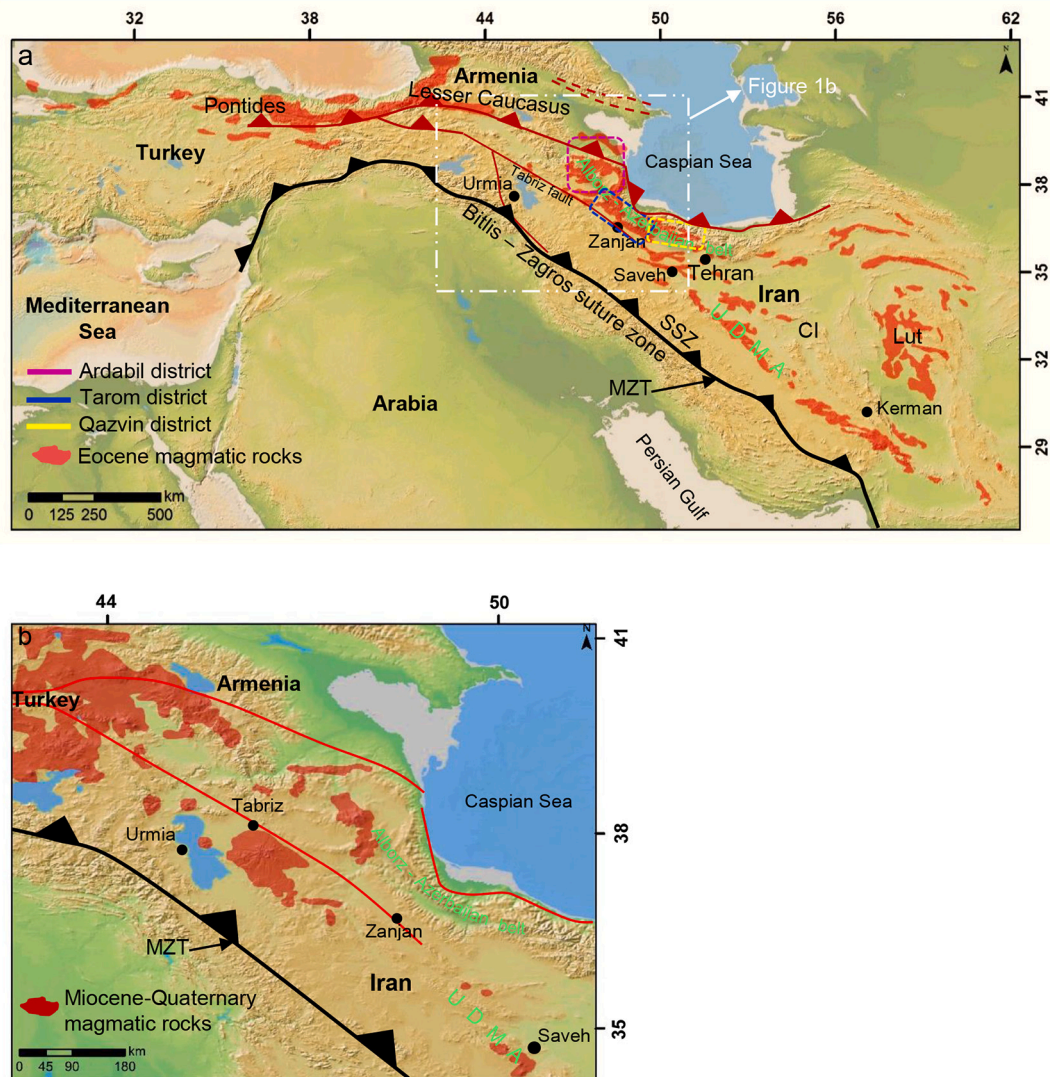


Fig. 1. SRTM (Shuttle Radar Topography Mission) images depicting (a) the Eocene magmatism along the UDMA and Alborz-Azerbaijan towards Armenia and Turkey and (b) the Miocene-Quaternary magmatism in NW Iran and neighbouring areas. Abbreviations are UDMA: Urmia-Dokhtar Magmatic Arc, CI: Central Iranian terrane, SSZ: Sanandaj-Sirjan zone, MZT: Main Zagros thrust.

Alborz Mountains, with the aim to provide further constraints on plate tectonic processes that are responsible for the Eocene high-flux magmatic event. We address several outstanding questions: (1) Why does the UDMA not continue towards Urmia but instead continues further north, along the Alborz Mountains, at greater distance from the trench? (2) What was the origin of voluminous high-K magmatism along the Alborz? (3) How do the Eocene and Miocene lavas differ in geochemical composition in the Alborz and UDMA? and (4) What were the magmatic cooling and exhumation rates from the Eocene to the Miocene in the Alborz Mountains?

2. Regional geology

The Alborz Mountains are located between the Caspian Sea to the north and the Central Iranian terrane to the south. They extend westwards into the Lesser Caucasus Mountains (Azerbaijan and Armenia) and further into the Pontides Arc (Turkey) and eastward into the Koppeh Dagh (Turkmenistan, Afghanistan; Fig. 1 a). Present-day shortening and intracrustal deformation in the Alborz Mountains are related to ongoing Arabia–Eurasia convergence (e.g., Vernant et al., 2004; Masson et al., 2007).

The stratigraphic succession of the Alborz ranges from the late

Neoproterozoic to the Holocene, and reaches a thickness of 12 km (Zanchi et al., 2009). The late Neoproterozoic siliciclastic Kahar Formation and the Lahijan granitic pluton (ca. 550 Ma; Hassanzadeh et al., 2008; Etemad-Saeed et al., 2016) are the oldest rock units outcropping in the Alborz. Paleozoic volcanic strata, including early Ordovician, Silurian and Devonian lavas and pyroclastic sequences, are found mostly along the western Alborz (Davies et al., 1972), whereas Mesozoic volcanic sequences are minor in the Alborz Mountains (e.g., Doroozi et al., 2016).

Cenozoic (66–0 Ma) volcano-sedimentary units in the Alborz are analogous (in thickness and magmatic history) to those from the UDMA, with the older and most voluminous part of this sequence (Paleocene to Eocene; 66–34 Ma) showing a wide range of compositions. Paleogene (66–23 Ma) volcanic strata are interlayered with marine as well as continental sediments (Stöcklin, 1968; Förster et al., 1972; Hassanzadeh, 1993; Verdel et al., 2011).

In contrast to the western Alborz, where Eocene lava flows are more voluminous, pyroclastic strata prevail in the central and eastern Alborz. Eocene volcanoclastic and volcanic sequences in the western and central parts of the Alborz are part of the ca. 5000 m thick Karaj Formation (Asiabanha and Foden, 2012), and dominantly occur on the south-western flank of the Alborz. The Karaj Formation includes clastic

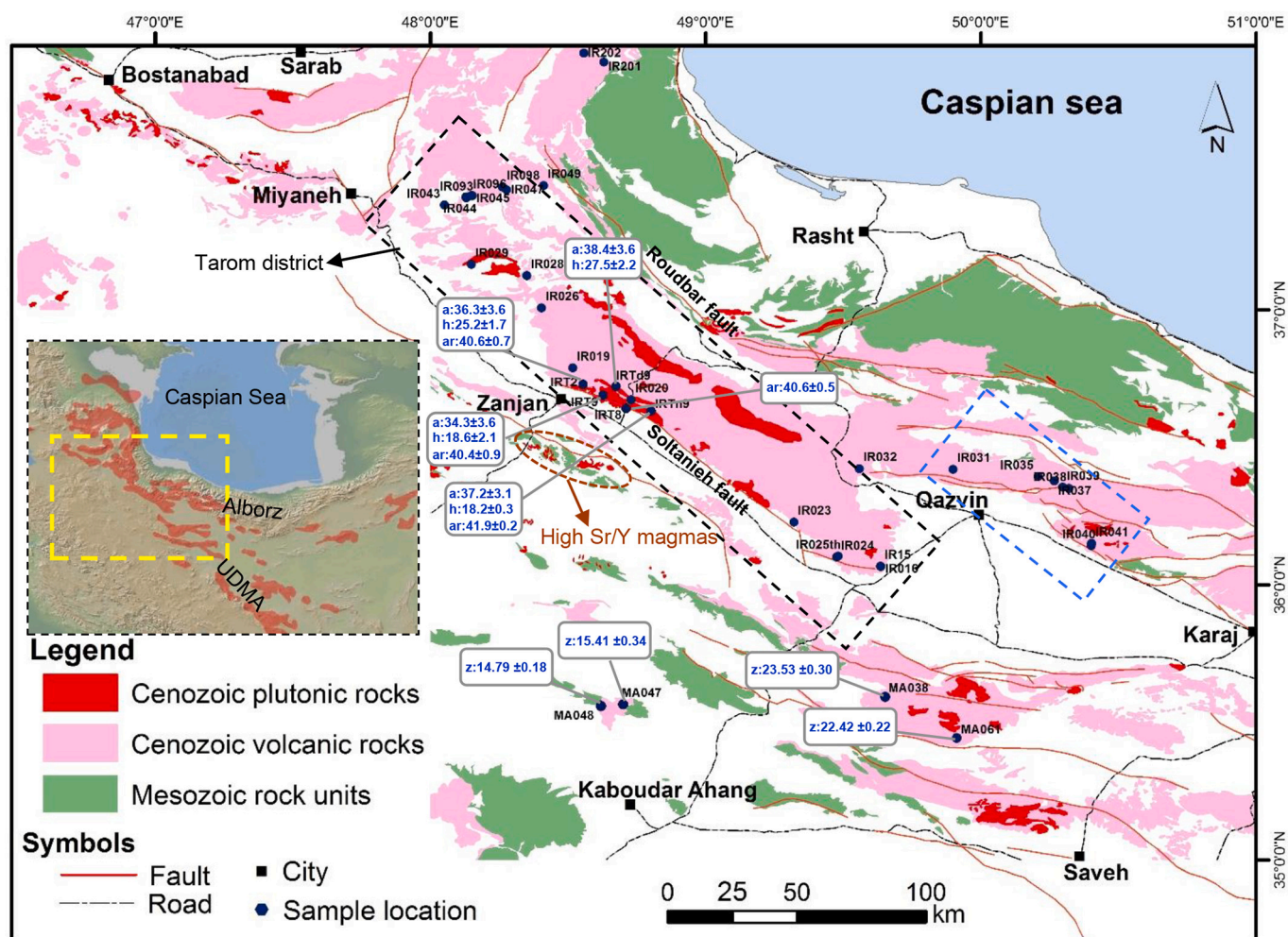


Fig. 2. Simplified geological map from the Tarom and Qazvin districts along the Alborz–Azerbaijan magmatic belt (modified after the 1:250,000 maps of Miyaneh, Zanjan, Bndar-Anzali and Qazvin-Rasht, Geological Survey of Iran). The Karaj Formation occupies most of the Cenozoic volcanic rocks on the map. The plutonic bodies (dominantly late Eocene) intruded into the Cenozoic volcanic strata. Black and blue dashed rectangles show the position of Tarom and Qazvin districts, respectively. The late Paleocene - early Eocene (ca. 56 Ma) high Sr/Y magmatism are after Nabatian et al. (2017) and Mokhtari et al. (2021). Age dating results including zircon ages (labeled by z), Ar/Ar age (labeled by ar), apatite fission track (labeled by a) and AHe ages (labeled by h) shown on the map. Insert showing the location of map on Fig. 1. (For interpretation of the references to colour in this figure legend, the reader is referred to the web version of this article.)

sedimentary and volcanoclastic deposits in the lower parts, and potassic calc-alkaline mafic to felsic lavas in the upper parts (Asiabanha and Foden, 2012). In general, Eocene magmatism along the Alborz Mountains is assumed to be accompanied by extension and subsidence, in order to account for the accommodation space for several kilometres of volcanic and volcano-sedimentary units of the Karaj Formation (Vincent et al., 2005; Rezaeian et al., 2012). Fault analyses and palaeostress reconstruction support Eocene extensional structures and normal fault kinematics along the Alborz Mountains (e.g., Zanchi et al., 2006; Guest et al., 2006; Yassaghi and Naeimi, 2011).

3. Outline of study area

Samples from Cenozoic (mostly Eocene) magmatic rocks in the Alborz Mountains were selected for detailed geochemical work (Figs. 2 and 3). We divide the samples according to their geographical position

from NW to SE into 3 groups, i.e., Ardabil district, Tarom district and Qazvin district (Fig. 1a). Detailed petrographic descriptions for the studied samples are presented in Supplementary File SM1 and Table S1.

Magmatism in the Ardabil district began in the late Cretaceous and intensified during the Eocene with voluminous mafic, intermediate and felsic lava flows and pyroclastic rocks (trachybasalts, basaltic trachyandesites and subordinate tephrite-basanite, phonolites, basaltic andesite, dacite and ignimbrite) of high-K calc-alkaline and shoshonitic affinities (Aghazadeh et al., 2011). Eocene magmatism was followed by the emplacement of Oligocene to Miocene (Fig. 1b) granitoid plutons and Plio-Quaternary volcanic rocks with within-plate geochemical signatures (e.g., Keskin, 2003; Kheirkhah et al., 2009). The Chehragh monzo-syenite (sample IR220) and Yuseflu granite (sample IR222) intruded into Eocene volcanic strata in the Ardabil district (Fig. 3).

The Tarom district is separated from Central Iran by the Soltanieh fault to the south and the Roudbar fault to the north (Fig. 2). The Tarom

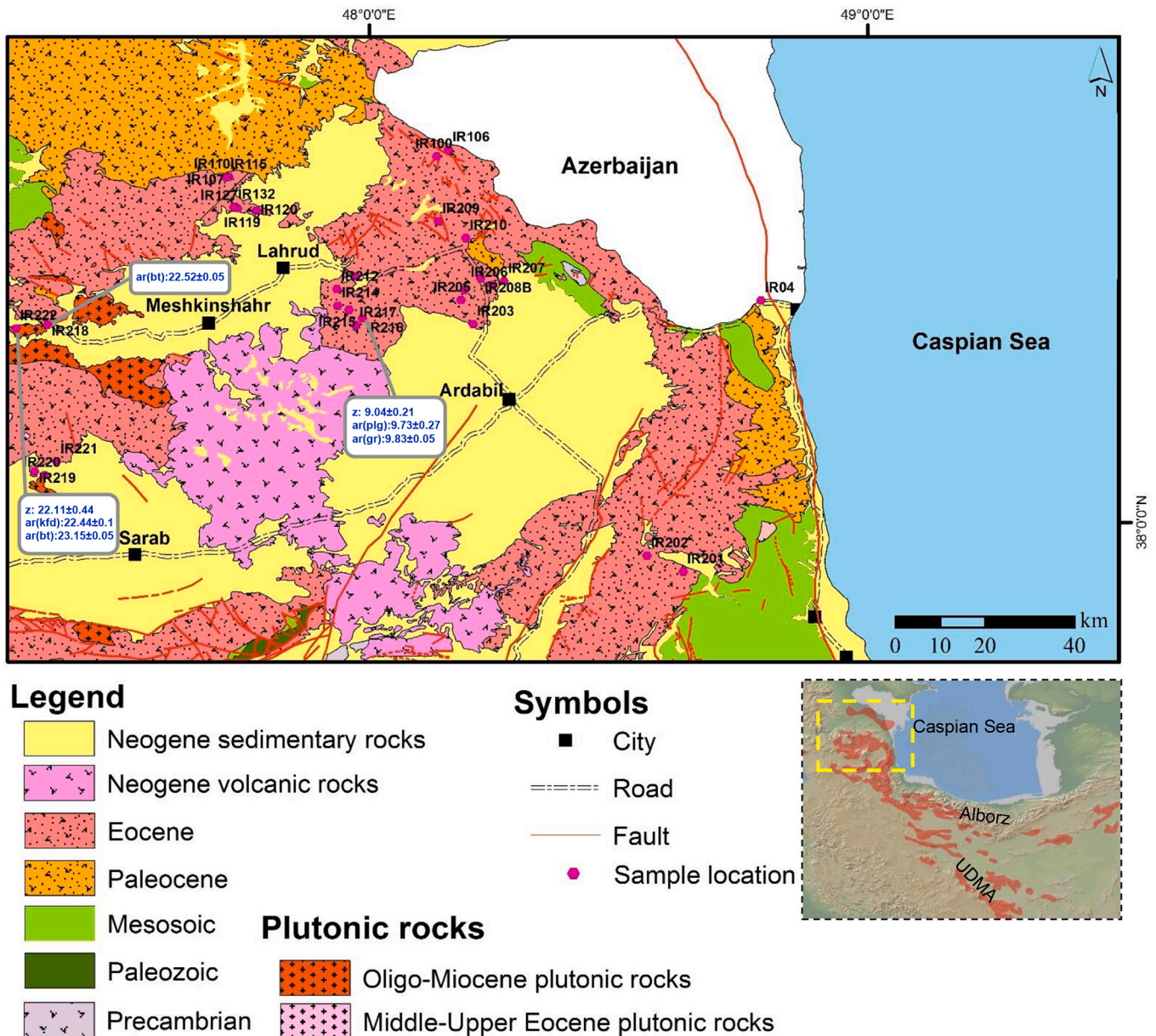


Fig. 3. Simplified geological map from the Ardabil district (modified after the 1:250,000 maps of Ardabil, Ahar, Bandar-Anzali and Miyaneh, Geological Survey of Iran). The Eocene rock units are predominantly composed of the Karaj Formation. The mid-upper Eocene shallow intrusions and Oligo-Miocene plutonic bodies intruded into the surrounding volcanic strata. Age dating results including zircon ages (labeled by z), Ar/Ar age (labeled by ar), apatite fission track (labeled by a) and AHe ages (labeled by h) shown on the map. Insert showing the location of map on Fig. 1.

district exhibits 30 to 40 km southward displacement compared to the overall trend of the Alborz belt. The structural elements and granitoid plutons in the Tarom area display dominant NW–SE trends (e.g., Nabatian et al., 2014, 2016a). Eocene lava flows and pyroclastic rocks prevail and are intruded by middle Eocene plutonic rocks (ca. 39 Ma; Castro et al., 2013; Nabatian et al., 2014, 2016a). The Eocene volcanic sequence shows evidence of submarine (early to middle Eocene) and subaerial (late Eocene) volcanism and includes pyroclastic and lava flows of trachyte, trachyandesite, andesite, basaltic andesite, olivine basalt, porphyritic and non-porphyritic rhyodacite compositions with

high-K calc-alkaline to shoshonitic affinity (e.g., Asiabanha and Foden, 2012; Nabatian et al., 2014, 2016a).

The Eocene volcanic units in the north of the Qazvin district (Fig. 2) are divided into two major groups (Asiabanha et al., 2009). The lower group comprises volcanoclastic units (~300–400 m thick) with two subfacies: pyroclastic green tuffs in the lower part and epiclastic tuffs and tuffaceous deposits in the upper part with evidence of explosive eruptions in a shallow marine basin. The upper group includes subaerial mafic to intermediate and locally felsic lava flows (Lasemi, 1992; Asiabanha et al., 2009). Faults in the Qazvin district show predominantly

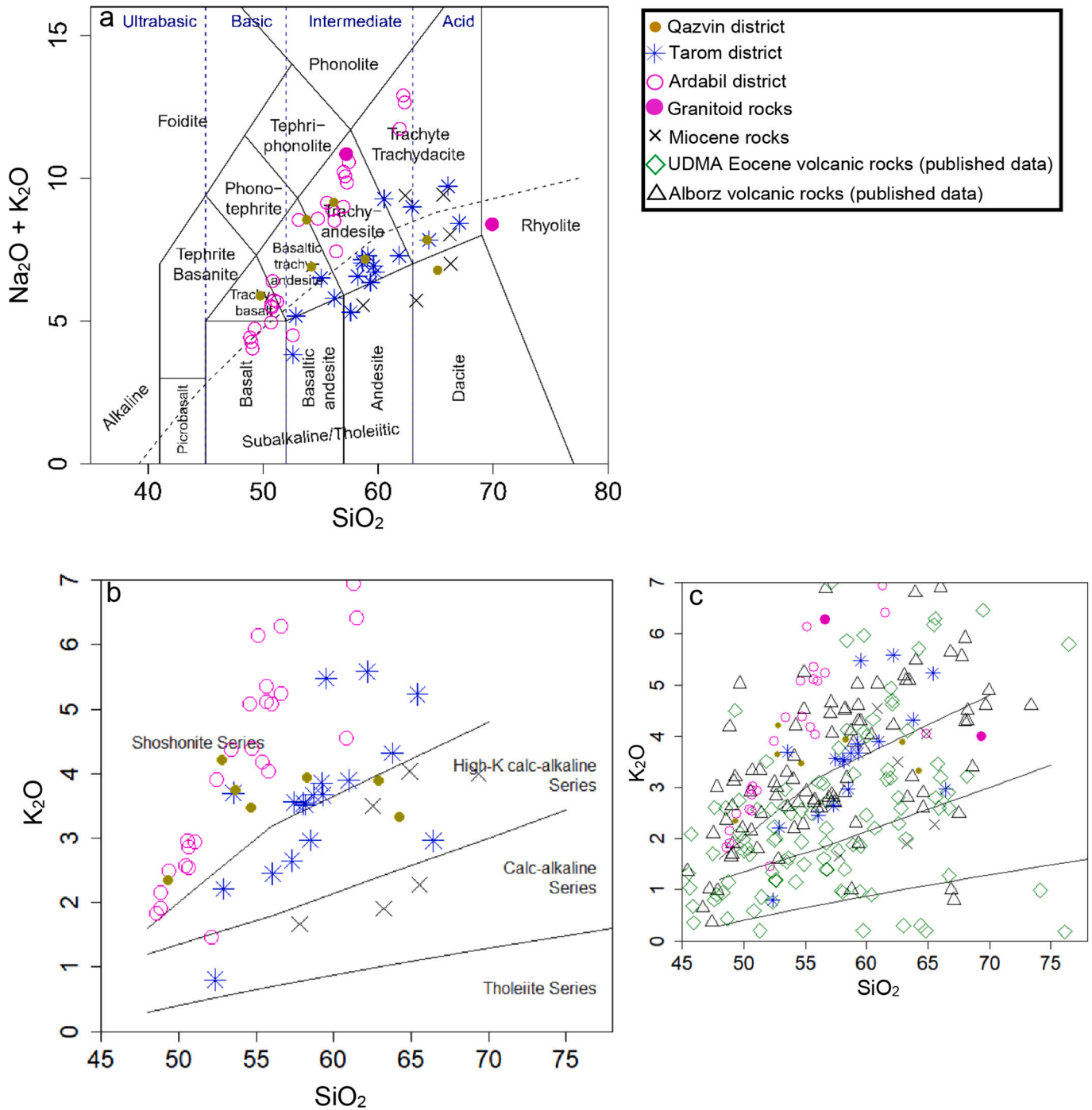


Fig. 4. (a) Whole rock geochemical classification diagram and (b) K₂O vs. SiO₂ discrimination diagram showing the composition and magmatic series of volcanic rocks along the Alborz magmatic belt, respectively. (c) K₂O versus SiO₂ diagram showing magmatic series of the Eocene igneous rocks in the Alborz – Azerbaijan compared to those from the UDMA. The reported bulk rock geochemical data from the Eocene volcanic rocks along the Alborz and UDMA are from Asiabanha and Foden (2012), Van der Boon (2017), Ghorbani and Bezenjani (2011), Kazemi et al. (2019) and Sarjoughian et al. (2019).

WNW–ESE trends. (Fig. 2).

In addition to the Alborz samples, four samples were selected from the northern part of UDMA, taken northwest of Saveh (MA-code samples; Fig. 2). These UDMA samples were taken in order to compare geochemical and geochronological signatures from both magmatic belts.

4. Analytical methods

53 samples from the Alborz and northern part of the UDMA were selected for whole rock geochemical analyses. Major and trace element compositions were measured at the Vrije Universiteit Amsterdam and Utrecht University, respectively. Ar/Ar geochronology on 3 samples from the Ardabil district was carried out at the Vrije Universiteit Amsterdam. Four samples from the Tarom plutonic body were selected for additional Ar/Ar data together with apatite fission track (AFT) and apatite (U-Th)/He (AHe) dating at the Salzburg (Ar/Ar and AFT dating) and Göttingen (AHe dating) Universities. Among all studied samples, there were only 6 magmatic rocks (4 samples in the UDMA and 2 samples in the Alborz-Azerbaijan belt) that contain zircon mineral for zircon U-Pb and Hf isotope studies. The zircon isotopic data were provided at the Institute of Geology and Geophysics, Chinese Academy of Sciences (IGGCAS). Detailed descriptions of analytical methods for all analyses are presented in Supplementary File SM2.

5. Results

5.1. Petrology and whole rock geochemistry

Major and trace element compositions of samples are presented in Supplementary File S2. In the classification diagram of Le Bas et al. (1986), the Alborz lava samples plot mainly in the fields of basalt to trachyandesite, trachyte and trachydacite (Fig. 4a). The Chehragh (IR220) and Youseflu (IR222) samples (Ardabil district) are intrusive and thus have compositions corresponding to granite and monzonite. Most of the samples from the Ardabil district and some from the Qazvin district are of alkaline affinity, whereas those from the Tarom district dominantly display a sub-alkaline affinity (Fig. 4a). Most samples are classified as high-K calc-alkaline to shoshonitic, with those from the Ardabil district having the highest K₂O contents (K content is increasing in westward direction; Fig. 4b). A comparison of K₂O contents of Alborz and UDMA magmas is shown in Fig. 4c. The majority of Alborz magmatic samples indicate high-K calc-alkaline to shoshonitic affinity whereas those from the UDMA show wide range of low to high-K calc alkaline series. Interestingly, the magmatic samples from the northern UDMA, close to the Alborz Mountains (north of Saveh, Fig. 2; Van der Boon, 2017), shows a magmatic series that trends towards shoshonitic. All samples display light rare earth element (LREE) and large ion lithophile element (LILE) enrichment and heavy rare earth element (HREE) and high field strength element (HFSE) depletion equivalent to those

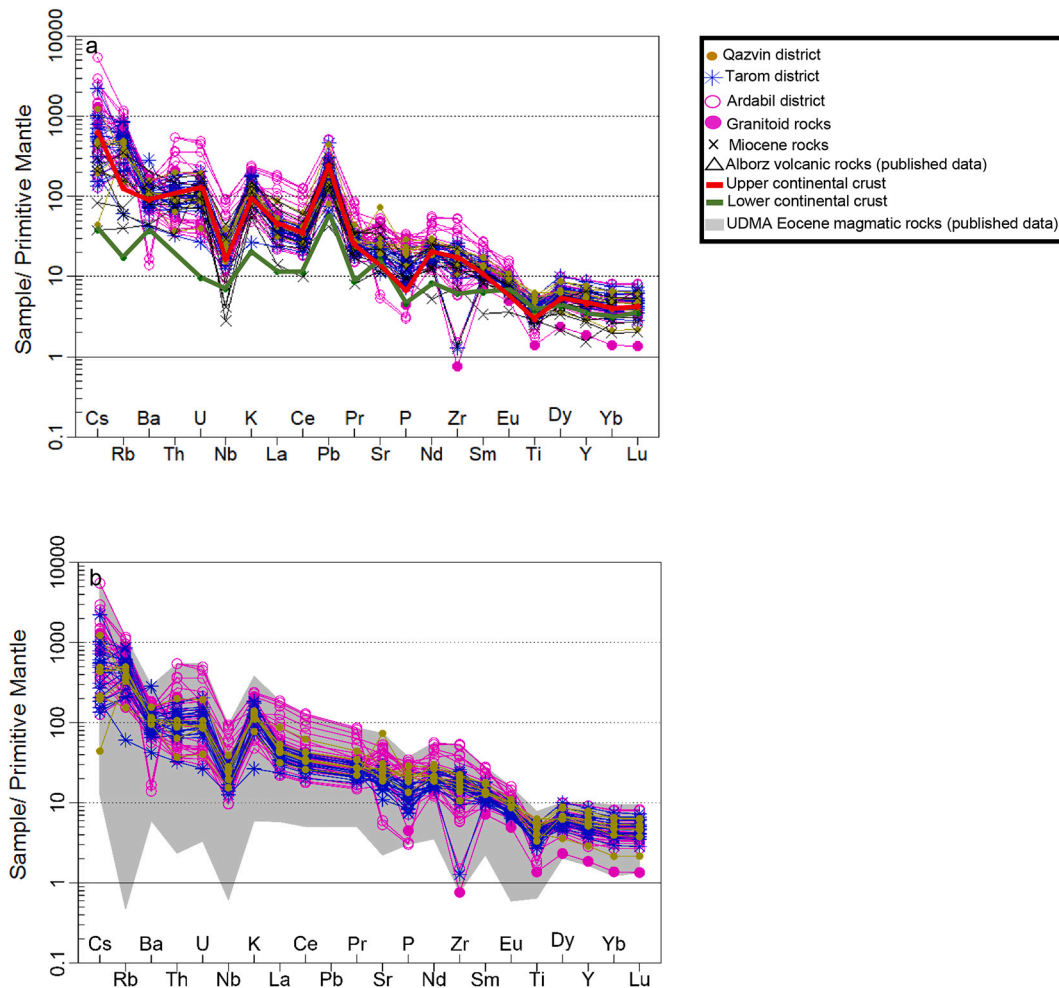


Fig. 5. (a) Primitive mantle-normalized (Sun and McDonough, 1989) trace element diagrams. The compositions of the lower and upper continental crust are after Rudnick and Gao (2003). (b) Comparison of trace element patterns from the UDMA Eocene magmatic rocks (shaded area; Van der Boon, 2017; Ghorbani and Bezenjani, 2011, Kazemi et al., 2019; Sarjoughian et al., 2019) with the Alborz lavas.

from the UDMA (Fig. 5a, b). Negative anomalies of Nb, P, Ti and Ba and positive anomalies of Rb, Th, U, K and Pb are present (Fig. 5a). Some differences are observed among the Alborz districts: For example, the samples from the Tarom and Qazvin districts show a larger depletion in HFSE than those from the Ardabil district. Except for a few samples, most samples do not show a striking anomaly for Sr. The samples from the Ardabil district reveal a larger variation of REE abundances than those from the Tarom and Qazvin districts (Fig. 6). All samples show a range of weak negative Eu anomalies ($\text{Eu}/\text{Eu}^* = 0.51\text{--}0.94$). In general, the trace element patterns of the Eocene magmatic samples from the Alborz-Azerbaijan belt are very similar to those from the UDMA.

5.2. U-Pb Zircon geochronology and Lu-Hf isotope data

Six samples (MA38, MA47, MA48, MA61 from the UDMA north of Saveh, and IR217, IR222 from the Ardabil district, Alborz) were selected for U-Pb zircon dating. Representative zircon CL images and U-Pb Concordia plots are shown in Figs. 7 and 8. Full LA-ICP-MS zircon U-Pb analytical data and Lu-Hf isotopic results are listed in Table S3 and S4, respectively.

5.2.1. Sample IR217

Zircons from sample IR217, a trachydacite, were found to typically display a pale orange hue. Crystal lengths range from ca. 60–300 μm and zircon aspect ratios vary in the sample from ca. 1:1 to 3:1. Several grains are fragmented but preserve oscillatory zoning (Fig. 7). Inclusions are prevalent. Most of the spots were selected from the zircon rims, but core analyses showed no age difference between the rims and the cores (Fig. 7). Fifteen measurements yield a range of $^{206}\text{Pb}/^{238}\text{U}$ ages from 7.9 to 9.7 Ma (Fig. 8). The weighted mean age of 9.04 ± 0.21 Ma (late Miocene; MSWD = 0.50) is used as the best estimate of crystallization.

The Lu-Hf isotopic results for sample IR217 are presented in Fig. 9. The $^{176}\text{Hf}/^{177}\text{Hf}$ ratios vary from 0.282924 to 0.283097, and initial Hf isotope ratios ($^{176}\text{Hf}/^{177}\text{Hf}$)_i range from 0.282924 to 0.283096. $^{176}\text{Yb}/^{177}\text{Hf}$ ranges from 0.0185 to 0.0561 (Table S4). As shown on the Hf isotopic evolution diagram of Fig. 9, the zircons have initial $\epsilon\text{Hf}(t)$ values of 5.6 to 11.7. The single-stage model age (T_{DM1}) of Hf isotopes (assuming that the magma or its precursor was derived from depleted mantle) for the analysed samples are 345–737 Ma.

5.2.2. Sample IR222

Sample IR222, a biotite-granite, was found to contain pale orange to colourless zircons. Crystal lengths range from c. 100–300 μm and zircon aspect ratios vary from ca. 3:1 (semi-elongated prismatic) to

approximately 1:1 (stubby). Most zircons preserve a well-defined oscillatory zoning and contain inclusions (e.g., zircon IR222–14; Fig. 7). In some cases, the zoned domains exhibit differences in their development, with uniform cores rimmed by finer oscillatory bands. Of the twenty analyses from this sample, one grain yielded an age of ca. 73 Ma (Late Cretaceous) and the others yielded a range of $^{206}\text{Pb}/^{238}\text{U}$ ages from 19.8 to 23.6 Ma. The young zircon grains yielded a $^{206}\text{Pb}/^{238}\text{U}$ weighted mean age of 22.08 ± 0.41 Ma (early Miocene; MSWD = 1.16) (Fig. 8).

The $^{176}\text{Hf}/^{177}\text{Hf}$ ratios of sample IR222 were found to range from 0.283000 to 0.283088, with initial Hf isotope ratios ($^{176}\text{Hf}/^{177}\text{Hf}$)_i from 0.282999 to 0.283088 (Table S4). The $^{176}\text{Yb}/^{177}\text{Hf}$ ratios range vary from 0.0132 to 0.0366 (Table S4). As shown on the Hf isotopic evolution diagram (Fig. 9), the zircons have initial $\epsilon\text{Hf}(t)$ values of 8.5 to 11.6. The single-stage Hf isotope model age (T_{DM1}) was found to be 357–558 Ma.

5.2.3. Sample MA38

Sample MA38 (dacite) was found to contain a limited number of zircon grains. The grains have a pale pink hue, and some are colourless. Crystal lengths range from c. 80–200 μm , and zircon aspect ratios are dominantly ca. 2:1. Some of the grains were found to be fragmented, while others preserve oscillatory zoning (Fig. 7). There are variations in the development of zoned domains, as some grains show one large uniform central zone rimmed by much finer oscillatory-zoned bands. Some of the zircons display segments of homogeneously textured zircon appearing as transgressive patches. Two zircon grains yielded $^{206}\text{Pb}/^{238}\text{U}$ ages of 685 Ma and 732 Ma (not only cores but also rims of grains). The old age population is interpreted to represent xenocryst grains. Six $^{206}\text{Pb}/^{238}\text{U}$ ages were found to range from 22.1 to 25.3 Ma. The young age population yields a weighted mean $^{206}\text{Pb}/^{238}\text{U}$ age of 23.5 ± 1.3 Ma (late Oligocene; MSWD = 2.7; Fig. 8).

The $^{176}\text{Hf}/^{177}\text{Hf}$ ratios vary from 0.281663 to 0.283086, and initial Hf isotope ratios ($^{176}\text{Hf}/^{177}\text{Hf}$)_i range from 0.283000 to 0.283086 (Table S4). $^{176}\text{Yb}/^{177}\text{Hf}$ ranges from 0.0126 to 0.0257 (Table S4). The zircons show initial $\epsilon\text{Hf}(t)$ values of 8.6 to 11.6. The single-stage Hf isotope model ages (T_{DM1}) were found to be 360–556 Ma.

5.2.4. Sample MA47

Zircons in sample MA47 (dacite) were found to generally have a pale orange hue, with some showing a pale pink colour. Crystal lengths vary in size from ca. 80–400 μm , and zircon aspect ratios vary from ca. 1:1 (subhedral, stubby) to 5:1 (elongated prismatic). Most of the grains preserve well-defined oscillatory zoning, but some show convolute boundaries (Fig. 7). Crystals display segments of homogeneously

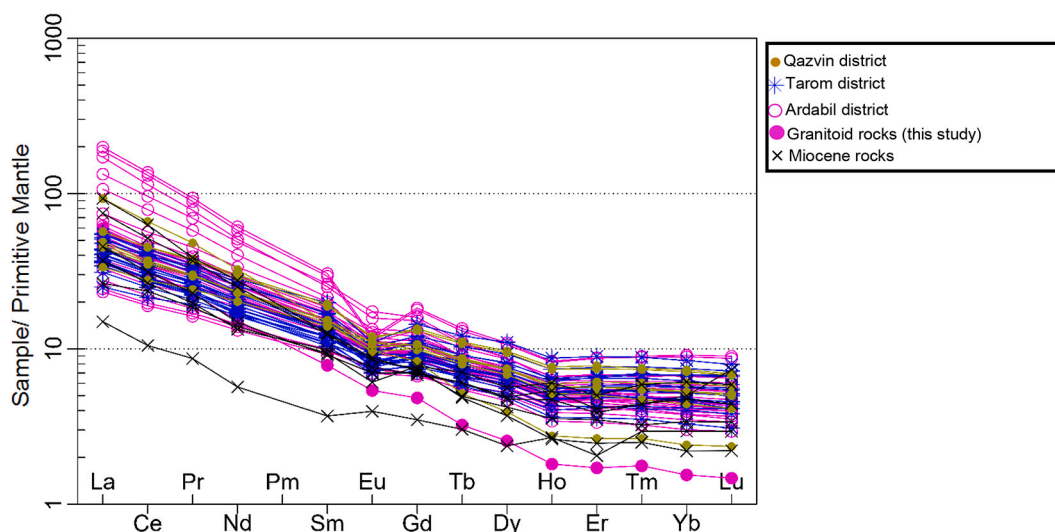


Fig. 6. Primitive mantle-normalized (Sun and McDonough, 1989) rare earth element (REE) diagrams of the studied samples.

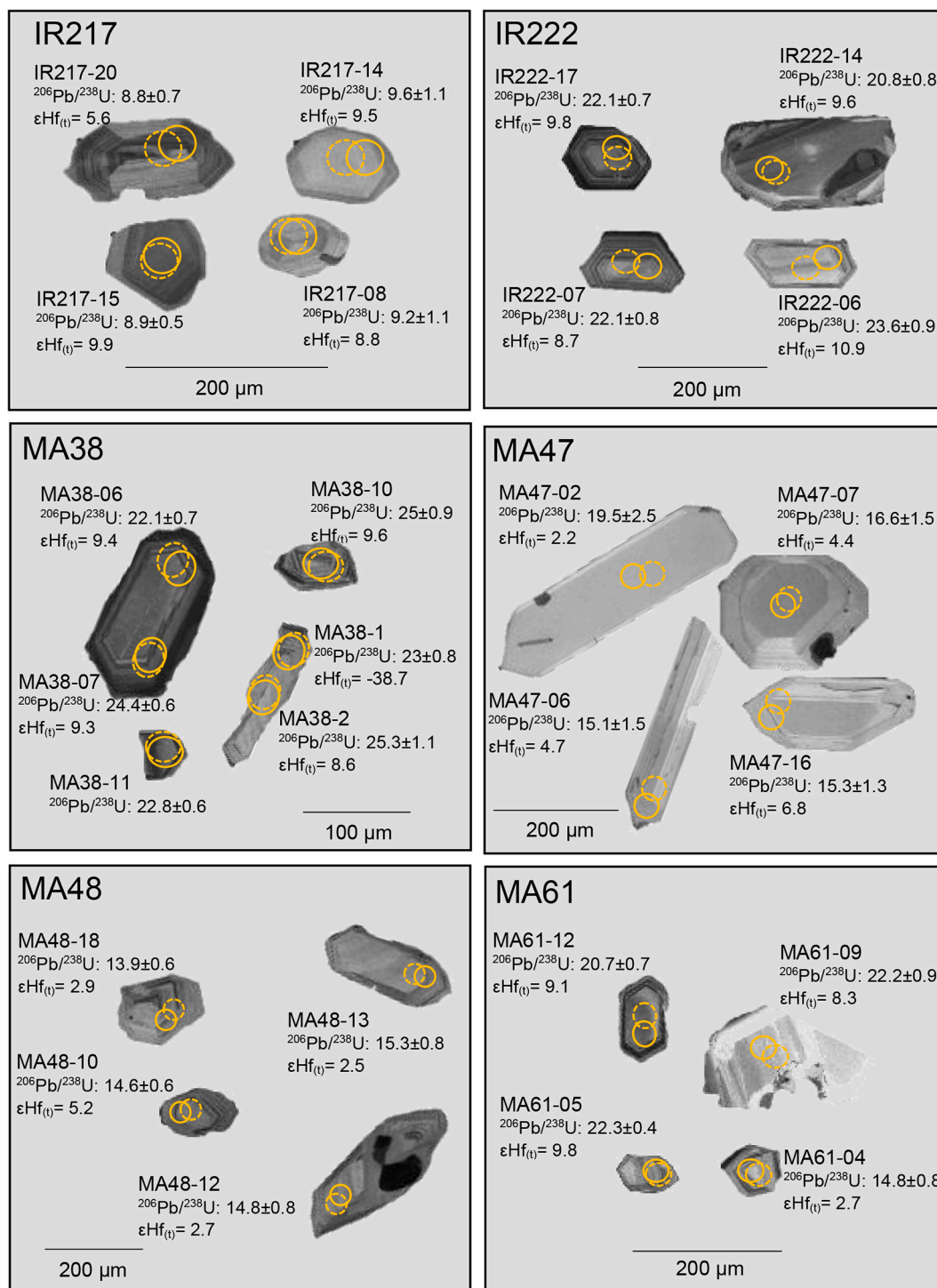


Fig. 7. Cathodoluminescence (CL) images of representative analysed zircons from the studied magmatic rocks. The dotted and solid circles show the Hf isotope and U-Pb dating analytical points, respectively.

textured zircon appearing as transgressive (across all pre-existing textures) patches and lobes. The analysed zircons yield a range of $^{206}\text{Pb}/^{238}\text{U}$ ages between 14.1 and 19.5 Ma and a weighted mean $^{206}\text{Pb}/^{238}\text{U}$ ages of 15.29 ± 0.66 Ma (MSWD = 0.75) (Fig. 8).

The $(^{176}\text{Hf}/^{177}\text{Hf})_i$ ratios vary from 0.282817 to 0.282955 (Table S4). The value range of $^{176}\text{Yb}/^{177}\text{Hf}$ is 0.0186–0.0631 (Table S4). The zircons show initial $\epsilon\text{Hf}(t)$ values of 1.9 to 6.8. The single-stage Hf isotope model ages (T_{DM1}) were found to be 663–974.

5.2.5. Sample MA48

Zircon grains in sample MA48 were found to vary from a pale orange to pale pink hue, whilst some are colourless. Crystal lengths range from ca. 120–400 μm , with the dominant aspect ratios being ca. 2:1 and 3:1, with some more equant grains present (Fig. 7). The zircons are prismatic while some of the grains are subhedral and fragmented. Most of the grains show a well-defined oscillatory zonation. Seventeen zircons were analysed, targeting rims and cores. No discernible age differences were observed between rim and cores with ages ranging between 13.9 and 15.3 Ma (Fig. 8), yielding an average age of 14.79 ± 0.35 Ma (middle

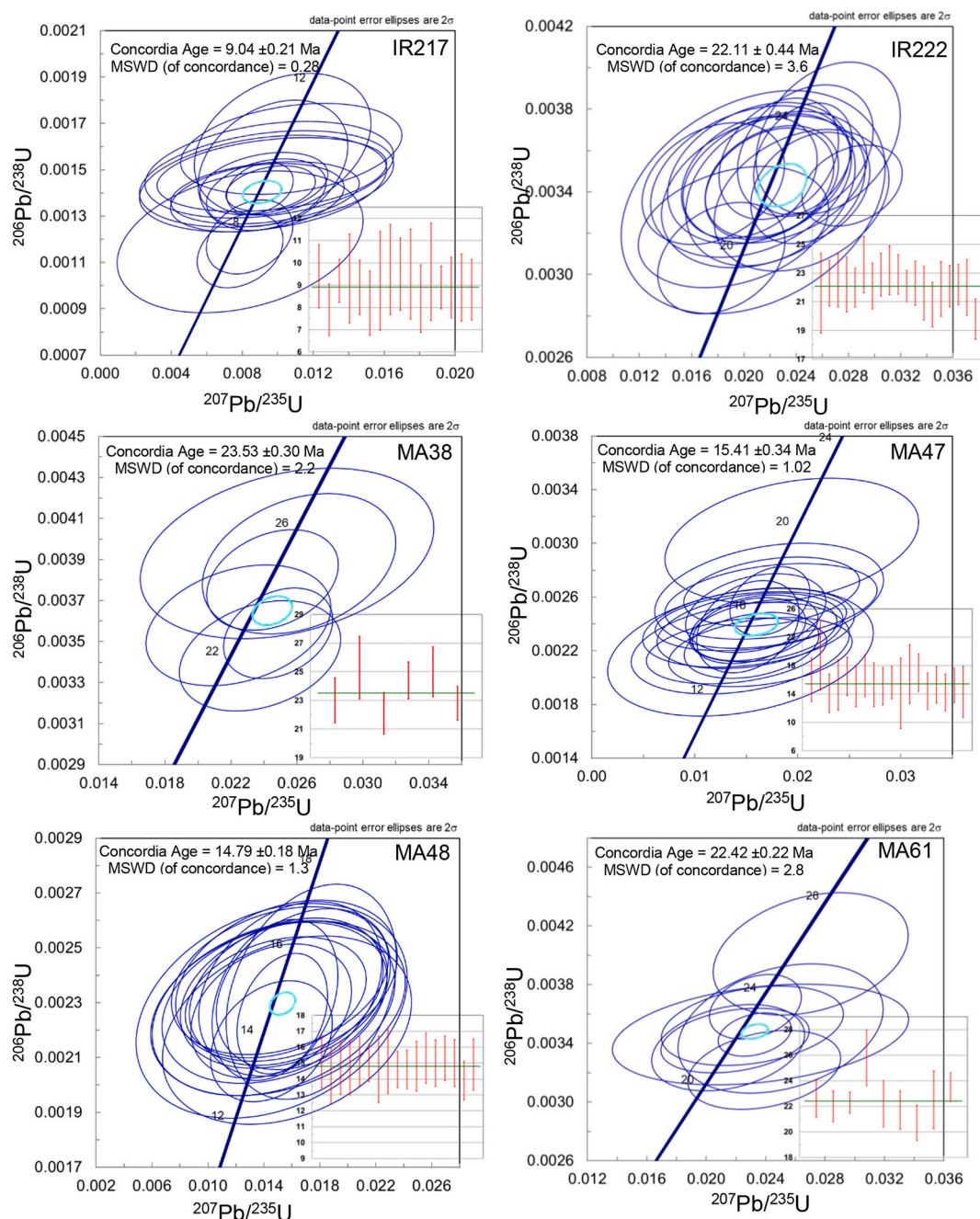


Fig. 8. U-Pb concordia diagrams for zircons from the studied magmatic rocks. The insert boxes show the average age diagrams.

Miocene; MSWD = 1.3; Fig. 8).

The $(^{176}\text{Hf}/^{177}\text{Hf})_i$ ratios vary from 0.282751 to 0.282952. The value range of $^{176}\text{Yb}/^{177}\text{Hf}$ is 0.0129–0.0362 (Table S4). The zircons show initial $\epsilon\text{Hf}(t)$ values of -0.4 to 6.7 . The single-stage Hf isotope model ages (T_{DM1}) for this sample were found to be 670–1123 Ma.

5.2.6. Sample MA61

Zircon grains in sample MA61 (trachydacite) were found to be predominantly colourless, with some grains exhibiting a pale orange hue. Crystal lengths range from ca. 60 to 260 μm , with the dominant aspect ratios being ca. 4:1 (elongated prismatic) to 1:1 (equant). Most of the zircons show oscillatory zonation and appear as fragmented grains in some cases. Some of the zircons show uniform cores being rimmed by finer oscillatory bands and some grains have convolute boundaries and patchy zones in CL images and a bright homogeneous texture. Ten

zircons were analysed, with preferentially targeted rims and subordinately targeted cores (Fig. 7). Nine zircon analyses show a range of $^{206}\text{Pb}/^{238}\text{U}$ ages between 20.7 and 25.8 Ma (Fig. 8). The weighted mean $^{206}\text{Pb}/^{238}\text{U}$ age is 22.40 ± 0.83 Ma (early Miocene; MSWD = 2.6) (Fig. 8). One zircon xenocryst indicates age of 714 Ma.

The $(^{176}\text{Hf}/^{177}\text{Hf})_i$ ratios vary from 0.282896 to 0.283079. The value range of $^{176}\text{Yb}/^{177}\text{Hf}$ is 0.0154–0.0683 (Table S4). The zircons show initial $\epsilon\text{Hf}(t)$ values of 4.9 to 11.4. The single-stage Hf isotope model age (T_{DM1}) was found to be 670–1123 Ma in this sample.

5.3. Ar/Ar dating

Two volcanic rocks (trachyte and trachyandesite; IR217, IR218; Ardabil district) and one intrusive rock from the granitic Youseflu pluton (IR222; Ardabil district) were selected for $^{40}\text{Ar}/^{39}\text{Ar}$ dating. The

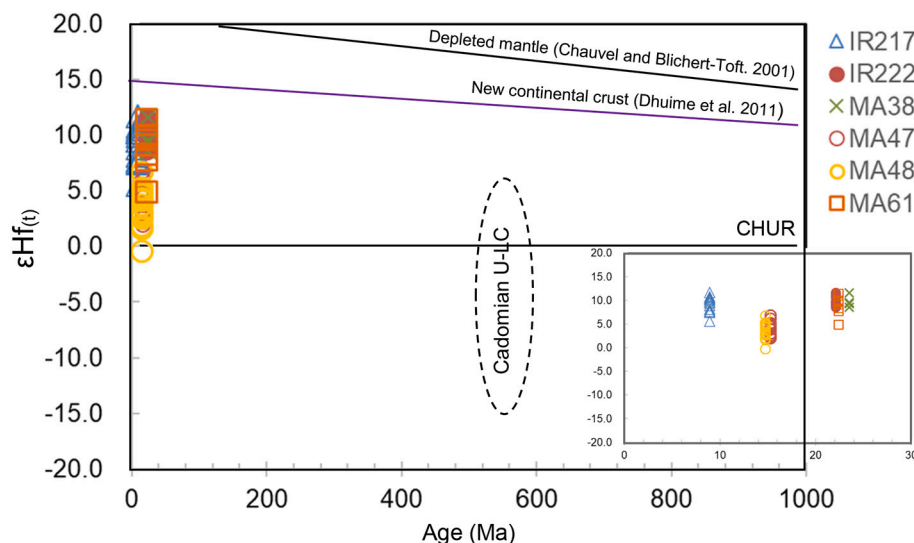


Fig. 9. $\epsilon\text{Hf}(t)$ vs. U-Pb age plot for zircons from the studied magmatic rocks. The average Cadomian upper-lower crustal composition also shown for comparison. The insert box shows the difference of Hf isotopes in the Miocene samples in detail.

locations of all samples are shown in Fig. 3. Age plateaus, single fusion analyses and isochron diagrams of samples IR217, IR218 and IR222 are displayed in Fig. 10 and compiled in Table S5. Plateau ages were obtained from sample IR217 (10.60 ± 0.33 Ma (plagioclase) and 9.67 ± 0.03 (groundmass)). Weighted mean fusion ages are obtained for IR218 (22.59 ± 0.04 Ma; early Miocene) and IR222 (22.48 ± 0.06 Ma (biotite) and 21.69 ± 0.08 Ma (alkali feldspar; early Miocene). The plagioclase of IR217 yielded one incremental heating spectrum of 9.73 ± 0.27 Ma (2 sigma analytical error) (Fig. 10; Supplementary File S5). A duplicate experiment failed, likely due to an experimental artefact or a source of extraneous ^{40}Ar is released at the higher temperature steps (Supplementary File S5). Two replicate experiments of the groundmass of this sample yielded 9.83 ± 0.05 Ma and 9.66 ± 0.02 Ma (Fig. 10). Isochrons are poorly constrained, but do not suggest the presence for excess argon (Supplementary File S5). The combined data suggest an age in the range of ca. 9.6–9.9 Ma for sample IR217. Seven fusion experiments of volcanic biotite IR218 yield a weighted mean age of 22.52 ± 0.05 Ma (Fig. 10). This overlaps with the intrusive feldspar age of IR222 of 22.44 ± 0.10 Ma. However, the IR222 intrusive biotite age of 23.15 ± 0.05 Ma is substantially older. If recoil effects play a limited role, this age difference suggest cooling from biotite closure temperature of 300 ± 25 °C (Harrison et al., 1985) through feldspar closure temperature of 200 ± 25 °C (Lovera et al., 1989) in roughly 0.7 Ma.

The samples from the plutonic rocks in the Tarom district yielded middle to late Eocene ages [IR-NT19: 36.9 ± 0.6 Ma to 40.9 ± 0.2 Ma (biotite), 40.3 ± 0.3 Ma (K-feldspar); IR-N19: 41.1 ± 0.3 Ma (K-feldspar); IR-N28: 35.3 ± 0.6 Ma to 42.1 ± 0.3 Ma (biotite), 38.0 ± 0.3 Ma (K-feldspar); IR-T52: 40.29 ± 0.41 Ma (biotite), 39.4 ± 0.2 Ma (K-feldspar)] (Fig. 11; Table S5), which are in agreement with the zircon U-Pb data reported from this pluton (Nabatian et al., 2014).

5.4. Low-temperature thermochronology

Four apatite fission track cooling ages ranging from 34.3 ± 3.6 Ma to 38.4 ± 3.6 Ma (middle to late Eocene) are reported for the Tarom samples in Table S6. Apatite (U-Th)/He (AHe) analyses were carried out for the same samples and AHe ages range from 18.2 ± 0.3 Ma to 27.5 ± 2.2 Ma (late Oligocene to early Miocene; Table S7).

6. Discussion

6.1. Fractional crystallization and crustal assimilation

The presence of clinopyroxene, plagioclase and olivine as phenocrysts in the majority of Alborz samples, coupled with the large range of MgO values (0.4–11.4 wt%; Table S2) suggests that these minerals were involved in extensive fractional crystallization prior to eruption. This is supported by correspondingly large ranges in Ni (1.9–134 ppm; one outlier with 260 ppm; Table S2) and Al_2O_3 values (13.9–21.3 ppm) indicating that most samples are more evolved than values expected for typical mantle-derived primary magmas formed in subduction zones (Ni = 100–300 ppm; $\text{Al}_2\text{O}_3 > 17$ wt%; e.g., Yao et al., 2018; Babazadeh et al., 2021). In addition to this, most of our trace element data from the Alborz belt plot between the fields for primitive mantle and the continental crust (Fig. 12a), with anomalies of elements such as Pb on primitive mantle-normalized trace element diagrams (Fig. 5a). This suggest involvement of crust either through crustal assimilation or sediment subduction and mantle source enrichment. Trace element ratios in the Alborz samples, such as Nb/Th (0.8–3.6 ppm), also lie between values reported for primitive mantle and continental crust (ca. 8 ppm – ca. 1.1 ppm, respectively; Taylor and McLennan, 1985; Rollinson, 2008). This is mirrored for La/Nb and Zr/Nb ratios that are another proxy for the involvement of crustal material (Thompson et al., 1984; Condie, 2005) (Fig. 12b, c, d). On further examination, the Pb and Sr contents for some of the mafic-intermediate samples in the Alborz belt are higher than those reported for average continental crust (ca. 17 ppm and 350 ppm, respectively; Taylor and McLennan, 1996; Rudnick and Gao, 2003) making it likely that an additional process beyond crustal contamination played a role in the compositional enrichment of these magmas. Furthermore, the lack of zircon (xenocrysts) in most of the Alborz mafic and intermediate magmatic samples (Table S1) suggests that zircon saturation has not been reached (Boehnke et al., 2013) and indicates that a low extent of contamination with felsic crust has affected the magmatic compositions. This evidence, however, should be treated with caution as the composition of crust might be heterogeneous and contain zircon-free assimilants.

By comparison, crustal contamination of mantle-derived melts can significantly decrease Ce/Pb ratios (Zeng et al., 2016) because the continental crust exhibits low Ce/Pb ratios (ca. 3.9; Rudnick and Gao, 2003). Overall descending trend of Ce/Pb ratio with increasing SiO_2 among the Alborz magmatic samples (with some outliers) suggest some

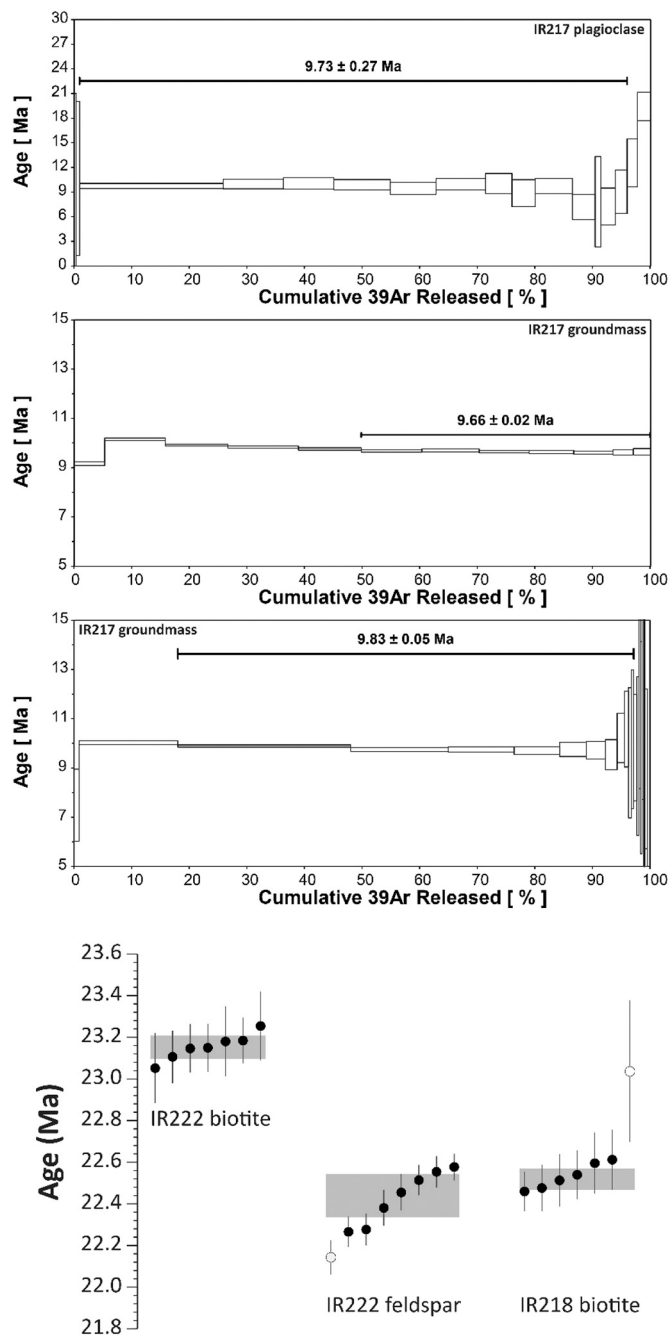


Fig. 10. $^{40}\text{Ar}/^{39}\text{Ar}$ geochronology data for magmatic rocks from the Alborz Mountains (Ardabil district).

degree of crustal contamination, especially upper crustal materials, across the area (Fig. 12e). The role of lower crustal contamination is likely insignificant, as most of the Alborz lavas are enriched in incompatible elements compared to the average lower crust whereas upper crustal components might have been contributed through magmatic evolution in some of the Alborz magmas (Fig. 5a). Basement rocks along the SSZ, UDMA and Central Iran are mainly composed of Ediacaran metamorphic and igneous rocks related to the Cadomian orogeny (e.g. Honarmand et al., 2016, 2018; Moghadam et al., 2018) which can be traced westward into Anatolia and SE Europe (Stern et al., 2021). These Ediacaran-Cambrian basement rocks of Iran and Turkey were exhumed from the middle - lower crust during the Cenozoic (Moghadam et al., 2018). A simple mixing model of most primitive magma in our data (sample IR2017) with the average composition of basement rocks in NW

Iran (Honarmand et al., 2018; Moghadam et al., 2018) shows that crustal mixing in high value rates (excess of 50%) is required to explain the trace elements chemistry of the Alborz basaltic and basaltic andesite lavas (Fig. SM3) which is unlikely given the mafic-intermediate nature of these magmas. This issue points to the source enrichment and melting conditions as the main factors controlled the chemical characteristics of the Alborz magmas. However, the role of upper crustal assimilation cannot be ruled out.

6.2. Insights into magma genesis and sources

High concentrations of incompatible trace elements (LILE and LREE) and significant negative Nb, P and Ti anomalies (Fig. 5a), as well as Zr/Y and Nb/Y (Fig. 13) ratios imply that the Alborz magmas were derived from fluid-modified melting of a lithospheric mantle source (Smith et al., 1999). High K_2O contents, relatively high MgO and enriched LILE and LREE all point towards a chemically enriched mantle source, which is commonly attributed to the addition of subducted components (e.g., Zindler and Hart, 1986; Beccaluva et al., 2004) and has been proposed for the Mediterranean and Iranian high potassium magmatism (according to the depleted mantle wedge model; Prelevic et al., 2010; Conticelli et al., 2009; Pe-Piper et al., 2014), or mixing of asthenosphere-derived magmas with subcontinental lithospheric mantle (SCLM) (e.g. Prelevic et al., 2010). Ratios of Zr/Y and Nb/Y (Fig. 13), corroborate the role of subduction-related petrogenetic processes (Condie, 2005) in the magmatic activity along the Alborz and UDMA. Sobolev et al. (2007) suggested that pyroxenites formed by reaction of eclogite-facies slab derived melts with mantle wedge peridotites can produce high-K magmas with high Ni (>450 ppm) but relatively low MgO (4.4–19.0 wt%) values, compared with magmas generated from mantle peridotites (Straub et al., 2008). The low contents of Ni in most of the Alborz primary lavas (less evolved melts) limit the role of partial melting of such pyroxenites in their genesis. Contamination of SCLM with slab derived materials has been inferred from the presence of blueschist facies metamorphic minerals (e.g., zoisite-epidote, lawsonite and phengite), which were derived from metamorphism of continental subducted sediments. Partial melts of such blueschist facies rocks can lead to magmas with high contents of K, Th, Sr, Rb, U and LREE (e.g., Conticelli et al., 2009). Mantle metasomatism resulted in the formation of hydrous mineral phases such as amphibole and/or phlogopite in the SCLM (Beccaluva et al., 2004; Mayer et al., 2013). The major elements of most primitive samples ($\text{MgO} > 5$ wt%) are comparable to those of experimental partial melts obtained from peridotites with hydrous phases (Couzinié et al., 2016 and references therein; Fig. 14a). Most of the Alborz samples show $\text{K}_2\text{O}/\text{Na}_2\text{O} > 1$, relatively low Ba/Rb (0.13–7.7; except for one sample with Ba/Rb = 14.9) and high Rb/Sr ratios (0.06–6.22), implying a phlogopite > amphibole-bearing mantle source (Furman and Graham, 1999) for the Eocene magmas in the Alborz. Our geochemical data suggest ca.1–8% partial melting of phlogopite + amphibole-bearing spinel + garnet peridotite (spinel < garnet; Fig. 14b) as the main source for most of the Alborz Eocene magmas, which is in agreement with a low degree of melting of enriched SCLM (phlogopite-amphibole-bearing lherzolite) proposed for the Eocene K-rich volcanism of the NW Iran (Moghadam et al., 2020; Nabatian et al., 2014, 2016a).

The Sm/Yb ratios of the UDMA samples point to higher and more variable degrees of partial melting (up to 20%; Fig. 14b). Higher Dy/Yb ratios along with variable La/Yb ratios in the Alborz samples (Figs. 14c) suggest larger contributions of deeper mantle material compared to the UDMA, as the Alborz source composition tends towards higher garnet contents (Fig. 14b). The low degree of partial melting of spinel+garnet (+ phlogopite > amphibole) peridotite suggests that the Eocene magmas in the Alborz Mountains are derived from the spinel-garnet transition at ca. 60–80 km (Robinson and Wood, 1998). The present depth of the lithosphere-asthenosphere boundary underneath the Alborz Mountains (ca. 90 km under Tarom district; Rahmani et al., 2019) is expected to be

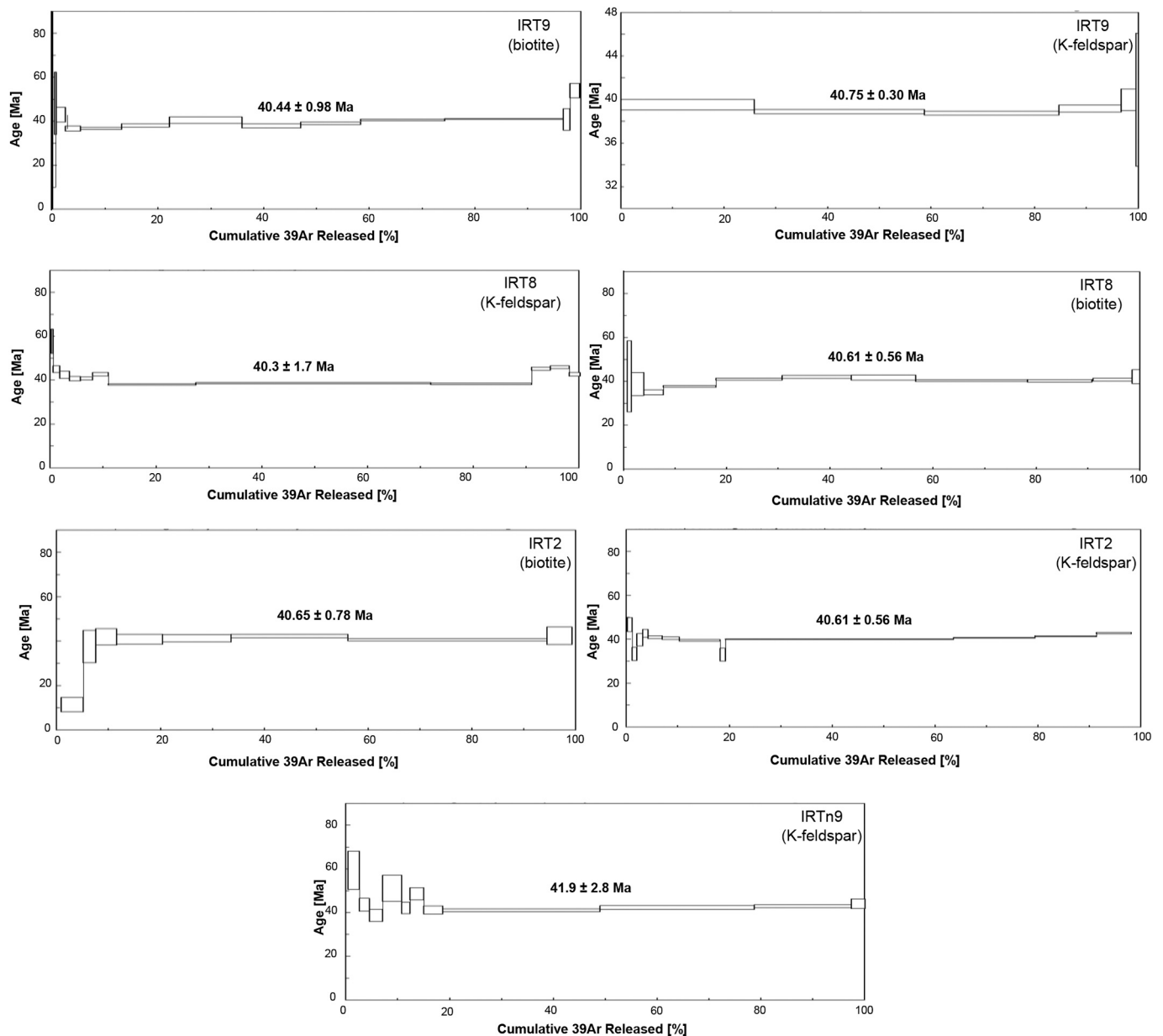


Fig. 11. $^{40}\text{Ar}/^{39}\text{Ar}$ geochronology data for the Tarom plutonic body (Tarom district), Alborz Mountains.

shallower during the Eocene subduction period (before Arabian-Iranian collisional thickening). Therefore, the Alborz lavas may have been generated from the contribution of both SCLM and asthenosphere reservoirs to the parental magmas.

6.3. Along/across-arc geochemical variation

6.3.1. Source characteristics

The Eocene Alborz magmatic rocks (e.g., Taki et al., 2009; Asiabanha and Foden, 2012; Nabatian et al., 2014, 2016a) generally contain lower abundances of H_2O -bearing minerals (e.g. amphibole and biotite) compared to similar Eocene igneous rocks from the UDMA (e.g., Ghorbani and Bezenjani, 2011; Ebrahimi and Tabatabaei Manesh, 2016; Taghipour and Mohammadi Laghab, 2014; Roshan and Nasr Isfahani, 2015; Shahriari et al., 2011; Sarjoughian et al., 2019; Kazemi et al., 2019) pointing to higher H_2O contents of UDMA magmas.

The higher values of K_2O as well Sr/Y and $(\text{La}/\text{Yb})_n$ ratios (Fig. 4, Table S2) in the Ardabil district compared to those from the Tarom and

Qazvin districts seem to be related to either modal fraction of garnet in the mantle source (e.g., Figs. 14a, b, d) or lower degrees of partial melting. Furthermore, the higher values of Ba/Rb and lower Rb/Sr in the lavas from the Qazvin district, compared to those from the Ardabil and Tarom districts imply higher contents of amphibole in their mantle source and suggest that the mantle beneath the Alborz Mountains is not completely homogenous and has compositional variation. Lanthanum content (a proxy for degree of partial melting or source enrichment) is more variable in the UDMA (e.g., Fig. 12b), even for the most primitive samples (UDMA: $\text{La}/\text{Nb} = 1.6\text{--}11.8$; Alborz belt: $\text{La}/\text{Nb} = 1.4\text{--}3.2$). This means that the degree of partial melting or the enrichment of the mantle source (heterogeneity of subcontinental mantle) in the UDMA was more variable in comparison with the Alborz. These patterns mirror a diminished extent of melting in the Alborz belt, because of a lower fluid flux from the slab as a function of distance to the trench or a less depleted mantle source underlying the Alborz Mountains (Fig. 15a; $\text{Nb}/\text{Yb}_{\text{Alborz}} > \text{Nb}/\text{Yb}_{\text{UDMA}}$). Furthermore, the narrow range of Ba/La (Fig. 15b) in the Alborz Eocene magmas may point to a different

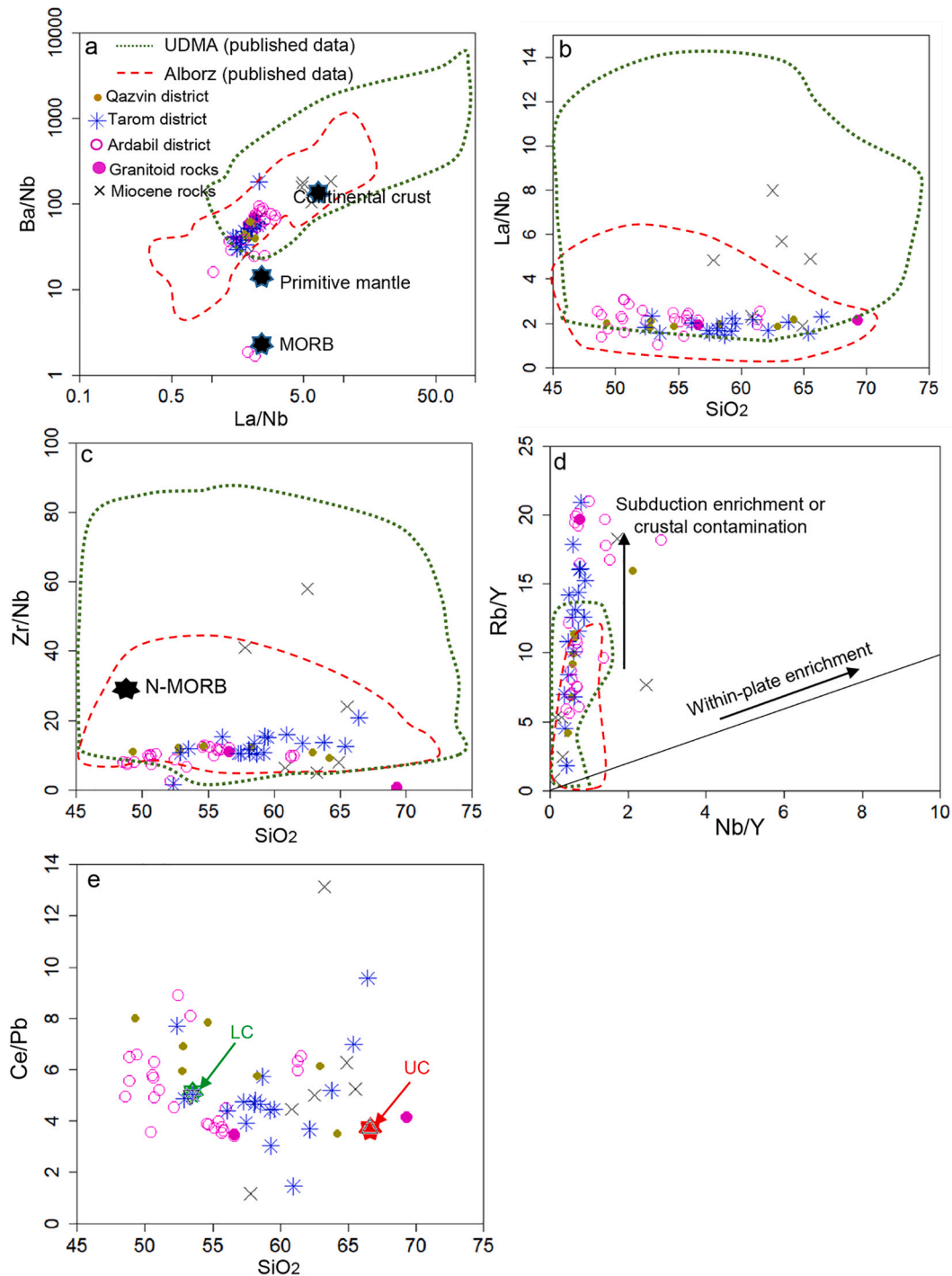


Fig. 12. (a) Plots of Ba/Nb vs. La/Nb for the Alborz and UDMA Eocene magmatic rocks (trace element values for the primary mantle and mid-ocean ridge basalt are after Sun and McDonough, 1989, the composition of continental crust is after Rudnick and Gao, (2003). (b) and (c) The variation of trace elements ratios (La/Yb and Zr/Nb) vs. SiO₂. The mean value of N-MORB (black star) is after Gale et al. (2013). (d) The variation of Rb/Y vs. Nb/Y for the magmatic rocks of the Alborz and UDMA. (e) Ce/Pb vs. SiO₂, the average compositions of lower crust (LC) and upper crust (UC) are after Rudnick and Gao (2013). The plot of the trace element ratios vs. SiO₂ provide the possibility to compare the trace variation in of the Alborz and UDMA samples (from basic to more evolved rocks) together.

mechanism of fluid delivery into the mantle wedge, with producing a more diffuse zone of partial melting. This condition is associated with low angle subduction and lower degree of partial melting (Saginer et al., 2013 and references therein) which is different from the “focused flux” of material from the steeper subducting slab. Lower degrees of partial melting in the Alborz are in agreement with higher values of (Sm/Yb)_N ratios and fluid-immobile elements (e.g., Zr, Y) in the Alborz magmas (Fig. 15c).

The pre-subduction conditions of the mantle wedge should also be considered as either highly depleted mantle or an old, enriched sub-continental lithospheric mantle. Lower values of Zr/Nb in the Alborz magmas (up to 30, with some exceptions) compared to N-MORB (Fig. 12c; Kirchenbauer et al., 2011), in association with scattered patterns (~2–50) and generally higher contents of Zr/Nb in the UDMA magmas (Fig. 12c), suggest pre-subduction enrichment of the mantle underlying the Alborz belt. Moreover, Fig. 15d illustrates a larger

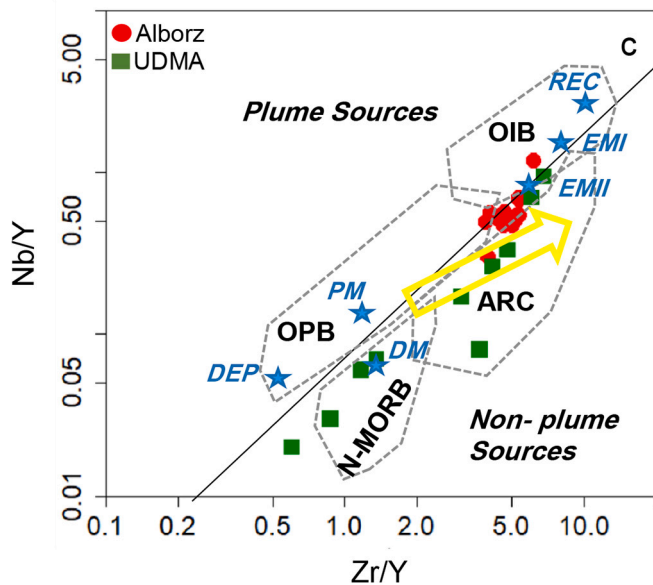


Fig. 13. (a) Nb/Y vs. Zr/Y (Condie, 2005) tectonic discrimination diagrams for Eocene magmatic rock along the UDMA and Alborz Mountains. The primitive magmatic rocks with MgO > 5 wt% were selected for comparison in the diagram which is analogous to the experimental high-K melts resulted from partial melting of amphibole, phlogopite-bearing lherzolite (Conceição and Green, 2004). The most primitive samples after Verdel et al. (2011) were added to the data source of the Alborz. The UDMA data are after Van der Boon (2017) and Sarjoughian et al. (2019). Arrow indicates effect of the subduction component. Abbreviations are as following: PM, primitive mantle; DM, shallow depleted mantle; EM1 and EM2, enriched mantle sources; UC, upper continental crust; ARC, arc-related basalts; N-MORB, normal mid-ocean ridge basalt; OPB, oceanic plateau basalt; OIB, oceanic island basalt; DEP, deep depleted mantle; EN, enriched component; REC, recycled component. (For interpretation of the references to colour in this figure legend, the reader is referred to the web version of this article.)

contribution of deep mantle material in the Alborz melts compared to the UDMA which dominantly follows the shallow component array. This context is supported by the higher values of Nb/Y (Fig. 13), suggesting a contribution of plume sources. As discussed below, the involvement of deeper mantle material in the Alborz lavas is not necessarily implied to deeper zone of magma generation but might be related to the addition of asthenosphere material to magma sources.

6.3.2. Slab components

Fluid-mobile and -immobile element ratios can be used to assess which slab component (fluid/melt) played a major role in melt generation. Our data shows that neither tracers of fluid addition (Pb/Ce, Ba/La, Ba/Nb, Ba/Th) nor the Th/La ratio (an indicator of subducted sediment involvement; Johnson et al. 2014) of the Eocene magmas show a systematic trend along the Alborz belt (Figs. 16, 15b), although the role of AFC process in modification of magma compositions should be considered. However, these ratios are more variable in the UDMA (Figs. 16a, b, c, d and 15b) implying a bigger role of slab material and water flux in partial melting beneath the UDMA. Furthermore, the Alborz Eocene magmas show more enrichment and sediment contribution in their mantle source than magmas from the UDMA (Fig. 16e).

The Alborz lavas have elevated Th/Nd with a minor increase in Ba/Nb ratios (with some exceptions from the Qazvin samples), whereas the lavas from the UDMA show more variable Ba/Nb ratios (Fig. 16f). This suggests a slab component, mainly consisting of hydrous fluid, as the main factor triggering higher degrees of partial melting beneath the UDMA. The Alborz lavas suggest sediment/alterd slab-derived melts as the main factor in metasomatizing mantle, but additional fluids are still necessary to allow the fluid-assisted partial melting of the slab

sediments.

6.4. Petrogenetic aspects of Miocene magmatic samples

Our new U-Pb data ascribes a Miocene age to a number of rock units previously mapped as Eocene (Stöcklin and Eftekhar-nejad, 1969; Eftekhar-nejad, 1987; Amidi, 1984; Figs. 2,3). These Miocene magmatic rocks include both, felsic to intermediate volcanic and plutonic rocks from the north-western Alborz as well as from the northern part of the UDMA (north of Saveh, Fig. 2). This finding underlines the necessity to obtain more radiometric ages to re-evaluate and refine the timing of Cenozoic volcanism along the UDMA and Alborz.

Geochemically, these Miocene rocks show low to medium Mg# (ca. 20–51) and trace element patterns analogous to those from other parts of the UDMA and Alborz. The Miocene samples have MgO < 3 wt%, SiO₂ > 56 wt%, Al₂O₃ > 15 wt% while some of these samples, especially those from the Alborz (IR-217, IR-218) show trends towards adakite-like compositions (La/Yb > 20, Sr/Y > 40). Late Miocene adakitic magmatism along the NW Alborz and UDMA (e.g., Omrani et al., 2008; Raeisi et al., 2021; Karimpour et al., 2021; Alirezai et al., 2017) has been attributed to slab break-off (e.g., Jahangiri, 2007; Omrani et al., 2008). The low to medium range of Mg# as well low Ni and Cr values imply a lower crustal origin for the studied Miocene rocks. The Miocene samples also show arc characteristics, similar to the Eocene samples along the Alborz and UDMA. This suggests that the arc-signature was still an influence on the source of magmas during the Miocene.

Furthermore, the zircon $\epsilon\text{Hf}(t)$ values of these rocks (Table S4) range from -0.4 to 11.7 (Fig. 9) suggesting involvement of older continental crust mixed with a juvenile component. Both Alborz and UDMA Miocene samples range from positive to slight negative $\epsilon\text{Hf}(t)$ with those from the Alborz around the upper limits of the range. Higher zircon $\epsilon\text{Hf}(t)$ of all studied Miocene samples compared to the $\epsilon\text{Hf}(t)_{(20\text{ Ma})}$ of Cadomian crustal rocks (e.g., Honarmand et al., 2018) imply involvement of juvenile melts. Zircon $\text{Hf}_{(\text{TDM}2)}$ model ages range between 0.35 and 1.1 Ga (Table S4), suggesting heterogeneity of the underlying crust along the Alborz and UDMA. The majority of samples show T_{DM} values comparable to Cadomian crustal fragments in Iran. Thus, partial melting of mafic to intermediate lower crust triggered by juvenile mantle derived melts is a possible origin for the Miocene magmatic rocks.

The Miocene has been suggested as a second flare-up episode along the Alborz and UDMA (e.g., Chiu et al., 2013) which volumetrically records less magmatism in Iran and succeeded the large Eocene (ca. 50–35 Ma) flare-up (Van der Boon et al., 2021).

6.5. Thermal-tectonic history

We used zircon U-Pb, ⁴⁰Ar/³⁹Ar dating, apatite fission track (AFT) and apatite (U-Th)/He to reconstruct the cooling history of Eocene intrusive bodies in the Tarom district.

The Tarom Eocene intrusions exhibit diorite to monzogranite compositions (Nabatian et al., 2014; Nabatian et al., 2016a) with medium- to coarse-grained porphyritic textures and clinopyroxene chemistry (Nabatian et al., 2016b), pointing to emplacement at shallow crustal levels. U-Pb dating of zircons yielded emplacement ages ranging from 39 to 42 Ma for these intrusive bodies (Nabatian et al., 2014). Zircon crystallization ages in agreement with ⁴⁰Ar/³⁹Ar ages of biotite (35.3 ± 0.6 to 40.29 ± 0.41 Ma) and alkali feldspar (38.0 ± 0.3 to 40.3 ± 0.3 Ma) imply very rapid cooling >> 100 °C/Ma following emplacement at a shallow crustal level. Post-emplacement cooling to ambient temperature along steep trajectories (Fig. 17) is followed by moderate cooling related to minor exhumation and unroofing of intrusive bodies from shallow crustal depths. This part of the cooling path is recorded by AFT (34.3 ± 3.6 to 37.2 ± 3.1 Ma; Table S6) and AHe data (18.2 ± 0.3 to 27.5 ± 2.2 Ma; Table S7) and (Fig. 17).

Integrating thermochronology data from various transects across the Alborz, Rezaeian et al. (2012) reported high exhumation rates from the

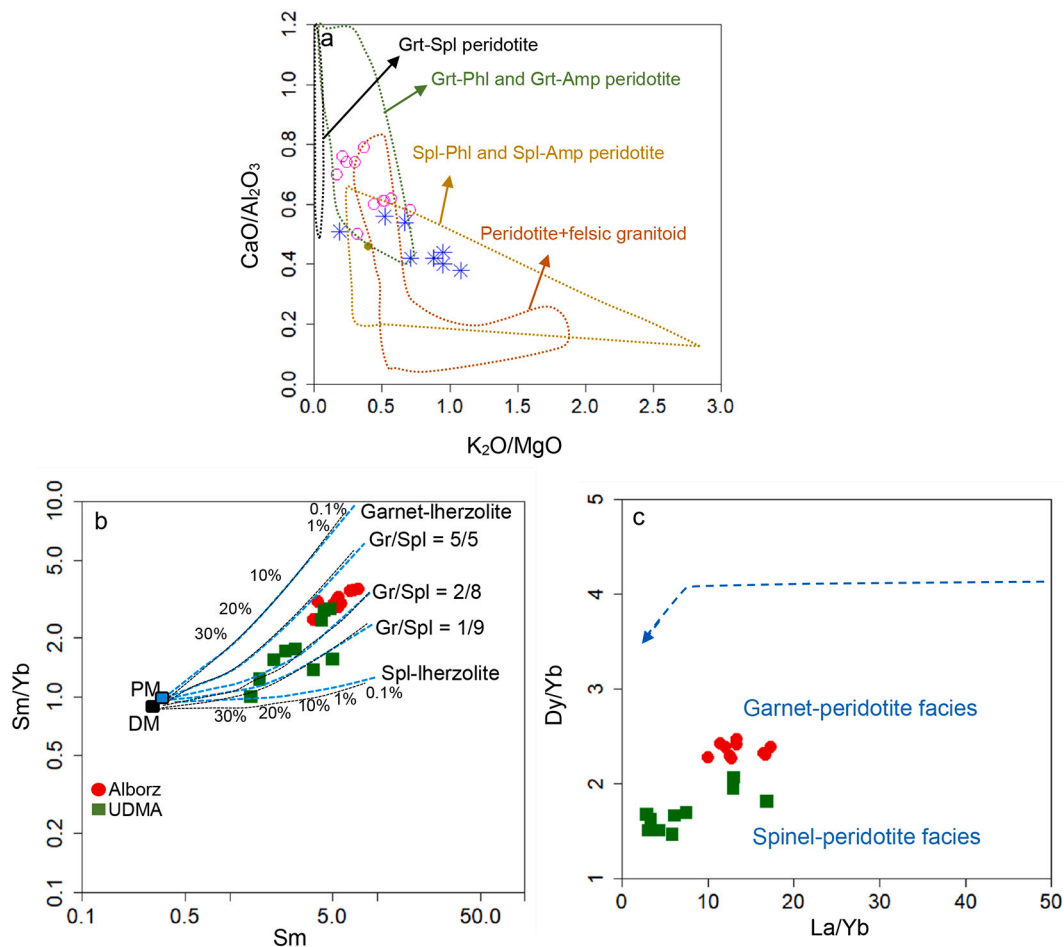


Fig. 14. (a) Comparison of major element ratios of the Alborz magmas ($\text{MgO} > 5$ wt%) with those of the experimental melts of metasomatized peridotites (Couzinié et al., 2016 and references therein). (b) and (c) Sm/Yb vs. Sm diagram for the most primitive Eocene volcanic rocks in the Alborz and UDMA. The data source are same as Fig. 13. The non-modal batch melting equations (Shaw, 1970) were used for calculation of melt curves (Wang et al., 2016). Dotted curves represent the melting trends starting from DM and PM sources with lithologies of garnet-lherzolite and spinel-lherzolite at 5:5, 2:8, and 1:9. Curves for spinel-lherzolite (with mode $\text{Ol}_{0.578} + \text{Opx}_{0.27} + \text{Cpx}_{0.119} + \text{Spl}_{0.033}$ and melt mode $\text{Ol}_{0.06} + \text{Opx}_{0.28} + \text{Cpx}_{0.67} + \text{Spl}_{0.11}$) and for garnet-lherzolite (with mode $\text{Ol}_{0.598} + \text{Opx}_{0.211} + \text{Cpx}_{0.076} + \text{Grt}_{0.11}$, and melt mode $\text{Ol}_{0.03} + \text{Opx}_{0.16} + \text{Cpx}_{0.88} + \text{Grt}_{0.09}$) are after McKenzie and O'Nions (1991) and Aldanmaz et al. (2000). The composition of DM (La, Sm, Yb = 2.50, 2.63, 3.05) and PM (La, Sm, Yb = 0.687, 0.444, 0.493) are after Sun and McDonough (1989). (d) and (e) La/Yb vs. Dy/Yb plot showing the depth of generation of Alborz and UDMA magmas (after Jung et al., 2006).

Middle Eocene to the Early Oligocene, followed by a phase of subdued exhumation during the Late Oligocene to Early Miocene. Exhumation intensified again in the Early Miocene lasting until the end of the Mid Miocene. Thermochronology data from the central and southern UDMA point to an increase of exhumation rates at ca. 20 Ma (middle-late Miocene) (François et al., 2014). Several causes have been suggested for the high exhumation rate around 35 Ma in the Alborz Mountains, such as the soft-collision of Arabia with Eurasia plates (Ballato et al., 2013) and Neotethyan back-arc extension and coeval magmatism (Vincent et al., 2005). However, the high exhumation rate could be related to a change in subduction geometry, as discussed in the next section

6.6. Geodynamic implications

6.6.1. Eocene magmatic flare-up

The Eocene is a time of high-flux magmatism in Iran (a flare-up; Verdel et al., 2011), with a significant peak around the middle Eocene (Van der Boon et al., 2021). Several causes have been suggested for this flare-up. Vincent et al. (2005) and Verdel et al. (2011) have argued that the flare-up was caused by an increase of the slab dip angle (e.g., slab retreat or slab roll-back), associated with subsequent asthenospheric upwelling. Moghadam et al. (2020) have made a case for extensional

tectonics in a back-arc/rear-arc setting for the Alborz-Azerbaijan volcanism. However, the main magmatic pulse in the Alborz (middle to late Eocene) is broadly contemporaneous with that of the UDMA and Lut block, suggesting a larger, regional trigger. Studies in other continental arcs have suggested that drivers for flare-ups are related to reorganisations of the subduction zone through events such as subduction of an aseismic ridge (De Silva and Kay, 2018), subduction erosion and tectonic shortening (Ducea and Barton, 2007) or episodes of arc deformation (Cao et al., 2015).

The geochemical signatures of the Alborz magmas can be explained by (I) upwelling of the asthenospheric mantle in a back-arc/rear-arc setting, possibly producing high-K calc-alkaline to shoshonitic magmas (e.g., Allen et al., 2003; Vincent et al., 2005; Verdel et al., 2011) or (II) bending or disrupting the subducting slab which leads to the displacement of arc magmatism. The slab bending/tearing process can produce both fore-to-back arc extension/transentation and mantle upwelling by toroidal flow around slab edges (e.g., Schellart, 2010; Gianni et al., 2019).

6.6.2. Implications for a viable tectonic model

Before evaluating any scenario, the conspicuous difference in distance to the suture zone between magmatic rocks in the Alborz and

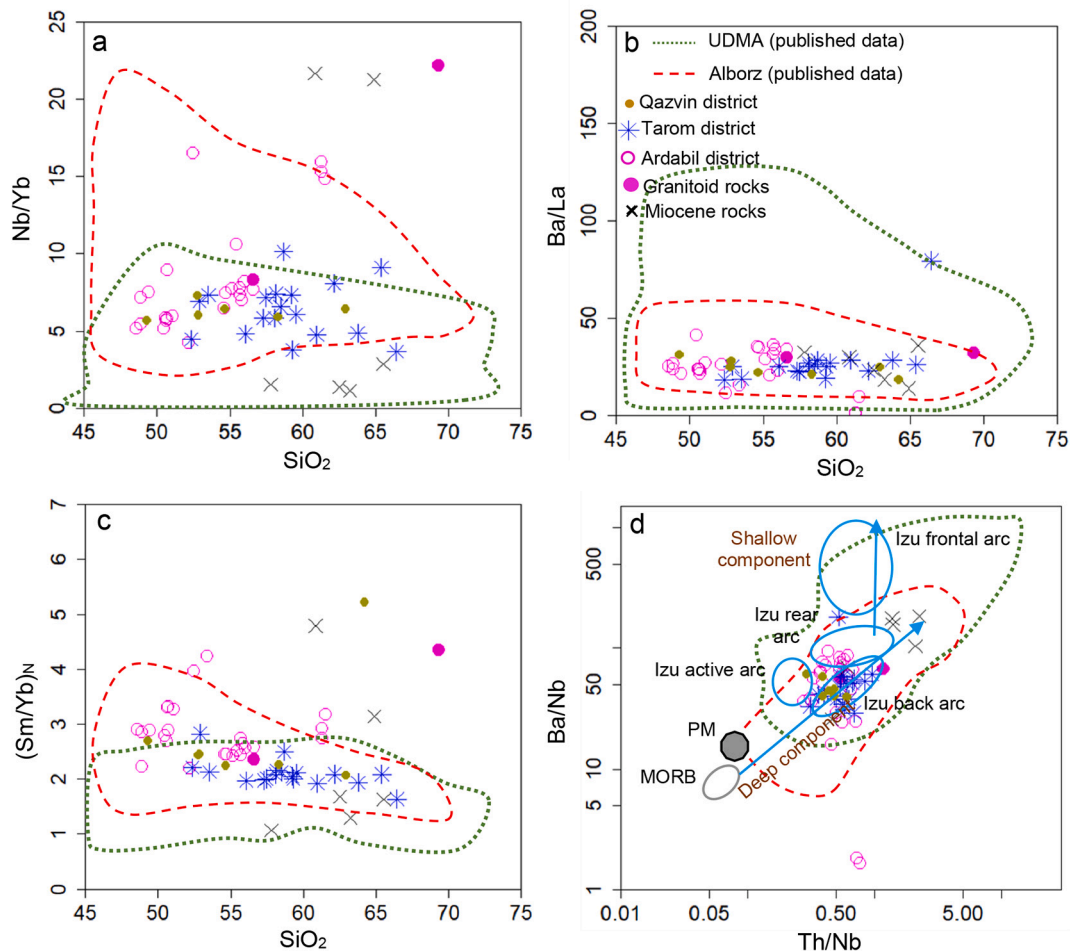


Fig. 15. Plots showing the Alborz and UDMA Eocene magmatic rocks on (a) Nb/Yb vs. SiO₂; (b) Ba/La vs. SiO₂, (c) (Sm/Yb)_n vs. SiO₂, (d) Ba/Nb vs. Th/Nb (data source after [Pearce and Stern, 2006](#)).

UDMA must be considered. Magmatic rocks in the UDMA have a distance to the suture zone of around 150 km, while the magmatic rocks in the Alborz are at a distance of around 250 km. These distances would be even greater considering the hinterland shortening after the Arabian–Iranian/Eurasia collision (~100–130 km post-collisional shortening) ([Morley et al., 2009](#); [McQuarrie and van Hinsbergen, 2013](#)). The inland position of the Alborz relative to the arc front (UDMA), contemporaneous flare-up in both the Alborz and UDMA, the distance between Alborz and Zagros suture zone and the results of recent seismic tomography (e.g., [Motaghi et al., 2017](#); [Chen et al., 2016](#); [Rahmani et al., 2019](#); [Stern et al., 2021](#)) combined point to a shallow dip subduction of the Neotethys slab beneath the northern part of the Iranian plateau, similar to the Makran area ([Motaghi et al., 2020](#)).

The geochemical signatures of the Alborz lavas are more consistent with an arc front than with a rear-arc setting. Rear-arc magmatic rocks are generally more primitive with greater LREE enrichments than those from the arc front ([Pearce and Parkinson, 1993](#); [Woodhead et al., 1993](#); [Miyazaki et al., 2020](#) and references therein). The contribution of slab-derived components to rear-arc melts is significantly lower in comparison with the arc front (e.g., [Ishikawa and Nakamura, 1994](#)). Assuming the Alborz as the rear-arc of the Neotethyan subduction system, the UDMA is expected to show more slab-derived enrichment that is not in agreement with the impressive similarity of Alborz and UDMA lavas (e.g. [Fig. 5](#)). Furthermore, rear-arc magmatism in a normal subduction system (i.e., without slab tear, slab gap) commonly occurs as a few smaller volcanic cross-chains or isolated plutons with lower magma production rates compared to the arc front (e.g., [Stern, 2010](#); [Guillot](#)

[et al., 2011](#); [Kuritani et al., 2008](#); [Kuritani and Nakagawa, 2016](#)). The voluminous magmatism along the Alborz-Azerbaijan belt during the Eocene is more compatible with an arc front setting than with a rear-arc setting. In the following, we try to address some key evidences.

If the UDMA is considered the only arc front of the Neotethyan subduction beneath Central Iran during the Cenozoic, this necessitates explaining the distinct change in the present distribution of Eocene magmatic rocks at the northern part of the belt (from south of the Zanjan area towards Urmia; [Fig. 1a](#)). According to the field observations and geological maps, the outcrops of Eocene volcano-plutonic rocks significantly decrease at the south of the Zanjan area wherein the significant volume of magmatism is observed in the north of this area, in the Tarom region along the Alborz belt. The “UDMA” thus does not continue towards Urmia in the Eocene, but instead goes further north, into the Alborz. [Van der Boon \(2017\)](#) and [Karimpour et al. \(2021\)](#) also pointed to a decline in magmatism south of Zanjan, northwest of the Saveh area, and replaced the “UDMA” by “Azerbaijan-Bazman arc” and “Saveh-Naein-Jiroft magmatic belt”, respectively. In addition, [Azizi and Tsuboi \(2021\)](#) has shown such sudden change in the Eocene magmatic exposures at northern part of the UDMA. The upwelling of hot asthenosphere due to Neotethys slab roll-back ([Azizi and Tsuboi, 2021](#))/slab lateral tearing ([Deevsalar et al., 2017](#)) has been proposed for occurrence of limited Paleocene-Eocene magmatic rocks in the northern SSZ.

There are several possible scenarios for this abrupt change in outcrop pattern of Eocene volcano-plutonic rocks, including:

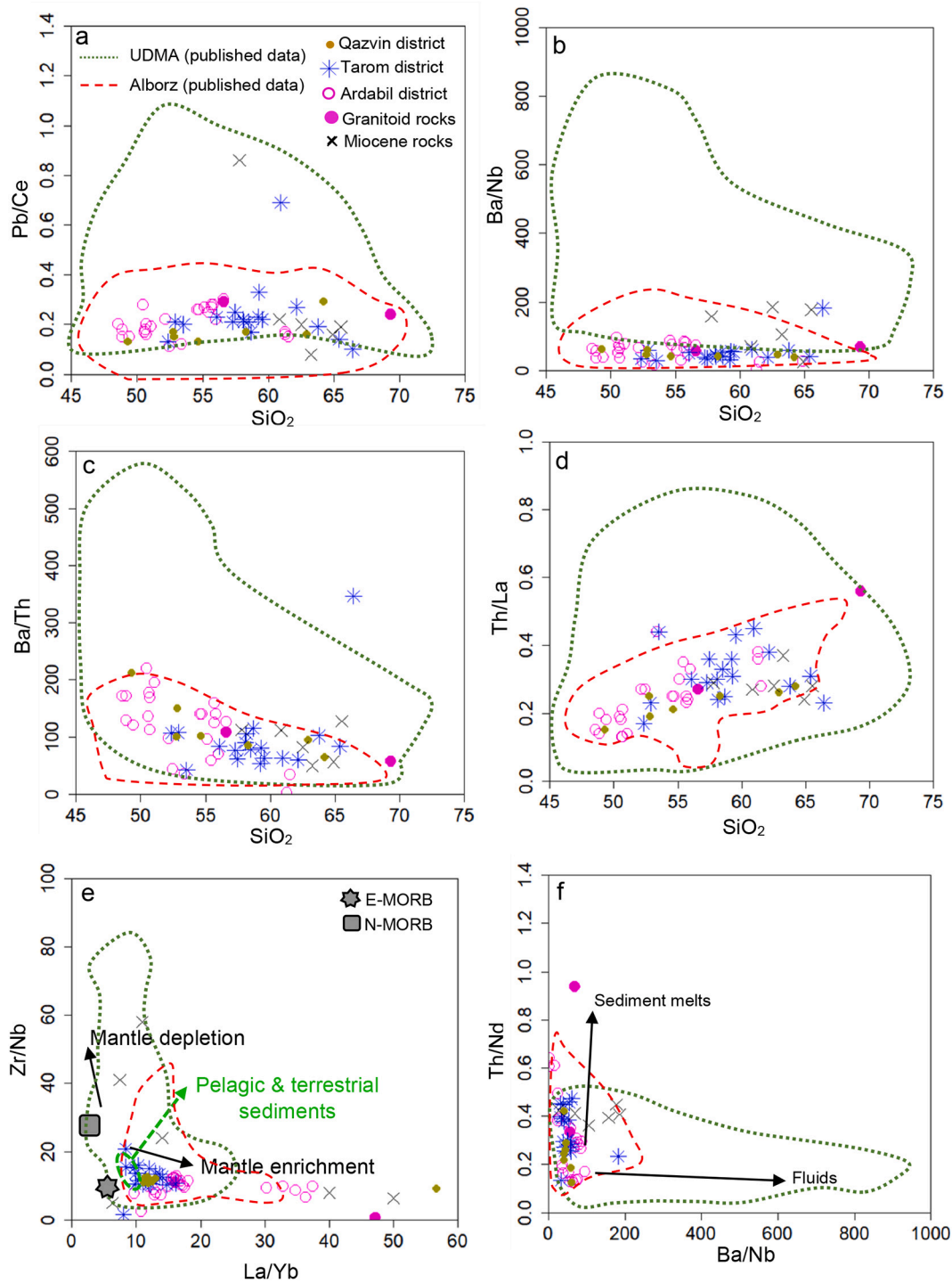


Fig. 16. Plots of (a) Pb/Ce vs. SiO₂, (b) Ba/Nb vs. SiO₂, (c) Ba/Th vs. SiO₂, (d) Th/La vs. SiO₂, (e) Zr/Nb vs. La/Yb, (f) Th/Nd vs. Ba/Nb.

- a) Erosion of the Eocene magmatic rocks: The Eocene sequence was deformed, uplifted, and eroded during the deposition of the Oligocene Lower Red Formation (Morley et al., 2009) so that the entire Eocene part of the UDMA between Urmia and NW Saveh (Fig. 1a) has been eroded away. However, there is currently no explanation for why erosion would only have affected this part of the volcanic arc, while leaving the rest of the arc relatively unaffected.
- b) Eocene volcanic rocks between Tafresh and Urmia are now covered by Neogene sediments (3–4 km thickness; Lotfi, 2001). This scenario is in contrast with aeromagnetic maps from the region. The UDMA shows a disruption at the northern part of this belt (northwest of

- Saveh) in aeromagnetic intensity maps (e.g., Teknik et al., 2019) and continues along the southern Alborz with strong magnetic anomalies like the ‘UDMA’. Similar variations have also been observed in the Bouguer anomaly maps (e.g., Tarverdizadeh, 2020) where the observed Bouguer anomalies at the south of the Zanjan area show a clear decreasing trend but become higher at the northern part (in the Tarom area, Alborz). Thus, we consider it unlikely that mechanisms a or b are the explanation for the lack of Eocene volcanics towards Urmia.
- c) Existence of a step in the arc front: Slab-bending/tearing has been reported from many subduction zones worldwide (e.g., Davaille and

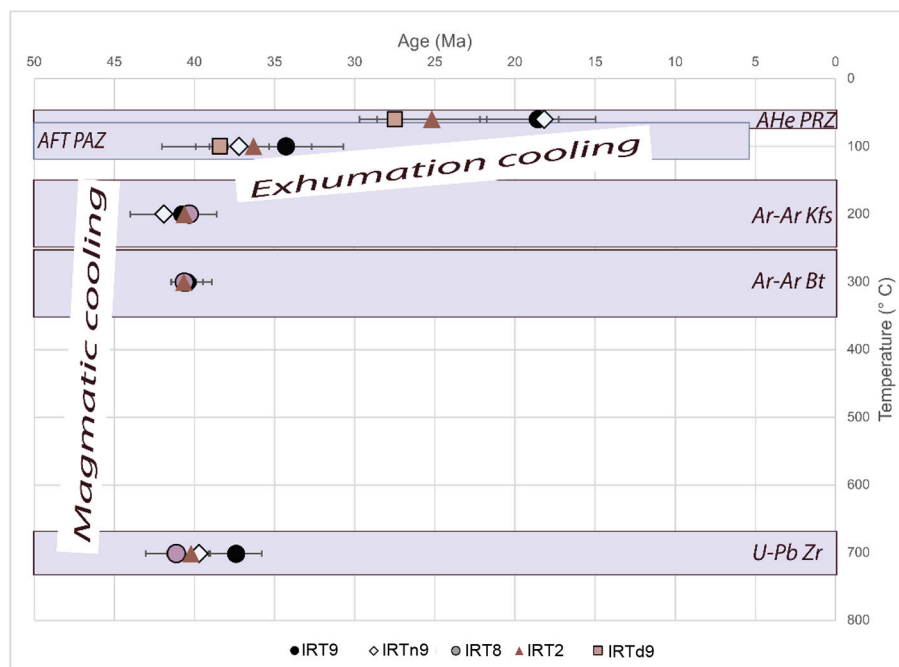


Fig. 17. Compilation of results from published U-Pb zircon geochronology (U-Pb Zr; Nabatian et al., 2014) and new Ar-Ar dating of biotite (Ar-Ar bt), K-feldspar (Ar-Ar Kfs), apatite fission track (AFT) as well as apatite (U-Th)/He (AHe) analyses for samples from the Tarom district. Post-emplacment rapid cooling is followed by exhumational cooling at moderate rates. A general zircon crystallization temperature of 700 °C was adopted for simplicity. The adopted closure temperatures for thermochronometers are as follows (Tc): biotite 300 ± 25 °C (Harrison et al., 1985); K-feldspar 200 ± 25 °C (Lovera et al., 1989), AFT partial annealing zone (APAZ) 60–120 °C (Fitzgerald et al., 1991) and AHe partial retention zone (PRZ) 40–80 °C (House et al., 1999).

Lees, 2004; Ferrari, 2004; Dimalanta and Yumul, 2008). Several factors may lead to changes in slab geometry, such as temporal-spatial variations in the buoyancy of subducting lithosphere (e.g., Royden and Husson, 2009), non-uniform slab roll-back (Cloos, 1993; Gianni et al., 2019), presence of mantle plumes (Murphy, 2016) or oceanic fracture zones (Georgieva et al., 2019) into the convergent margin, asymmetric distribution of subduction forces due to oblique subduction (Boonma et al., 2023). The transition between a flat to steep part of the slab is likely achieved through gradual slab bending or abrupt slab tearing (Liu and Pysklywec, 2023 and references therein).

The assumption of one single arc across Iran which underwent slab-bending/tearing northwest of Saveh and consequent change in location of the arc front might be a plausible model for the geodynamic evolution of Neotethyan subduction beneath the Iranian plateau during late Paleocene-Eocene times. The slab flattening led to a shift of the arc-front further away from the Zagros suture zone. Identification of vertical slab-bending/tearing in modern subduction zones is, however, much easier than old subduction systems, as the geological fingerprints are overprinted by collisional structural evidence. Slab tear processes are commonly associated with a change in trend of the arc front (Gianni et al., 2019), a local reduction in arc activity or arc shut-off and mantle-wedge flow changes and thermal perturbations (Govers and Wortel, 2005; Roche et al., 2018), voluminous magmatism with alkali and/or OIB-like affinity in the back of the arc front (e.g., Prelevic et al., 2015; Cocchi et al., 2017), magmatism with high Sr/Y and adakitic-like signatures (e.g., Hu and Liu, 2016), extension in the overriding plate (Jolivet et al., 2015) and enhanced exhumation of upper plate (especially above the shallow dipping slab; G erault et al., 2015; Castellanos et al., 2018; Kiraly et al., 2020).

The arc characteristics of the Alborz Eocene magmas along with dominant high-K to shoshonitic magmatism, variation in type of slab-derived components (higher sediment/altere slab-derived melts) compared to the UDMA magmas, more asthenospheric contributions in

the Alborz magmas; occurrence of the late Paleocene - early Eocene high Sr/Y and adakitic-like magmas (ca. 56 Ma; Nabatian et al., 2017; Mokhtari et al., 2021) south of Zanjan (Fig. 2) and a higher exhumation rate of the Alborz Mountains during the Eocene (e.g., Axen et al., 2001; Guest et al., 2006; Rezaeian et al., 2012; Ballato et al., 2013) compared to the UDMA, are all in agreement with a model that includes a change in slab geometry in the Neotethyan subduction system during the Eocene (Fig. 18). Furthermore, Rabiee et al. (2020) proposed segmentation of the lithospheric slab and asthenospheric upwelling for the Cenozoic magmatism in NW Iran. We thus consider it likely that the change in slab geometry that can explain the change in location of the volcanic arc front from the UDMA to the Alborz was accompanied by local tearing of the Neotethys slab. A slab tear model for Neotethyan subduction is also hypothesized based on a seismic compilation (Hafkenscheid et al., 2006). Hafkenscheid et al. (2006) show that there is a difference in extent of high velocity anomalies between northern and central parts of the UDMA in their tomographic sections. The cross-section tomographic images relevant to the northern part of UDMA, including the Alborz belt, indicate a more continuous high velocity anomaly than that of the central part of the UDMA (e.g., Hossein Shomali et al., 2011; Agard et al., 2011; Motaghi et al., 2017; Rahmani et al., 2019). This feature may point to a different evolution of the slab as the earlier slab detachment was beneath the central part of the UDMA than the northern part (e.g., Veisi et al., 2021). Furthermore, seismic imaging of the lithospheric structure beneath the Zagros orogenic belt (Paul et al., 2010) shows a lower angle of the Arabian-Eurasia suture fault zone in northern part of the Zagros collisional belt compared to the southern part, which may point to a lower angle of subduction in the northern part of the UDMA. Thus, all these studies imply a different evolution of the slab in the northern and southern parts of the UDMA.

A change in slab dip may have provided changes in thermal structure of the mantle wedge. This led to a change in the location of mantle wedge melting and the position of arc front. With these conditions, slab roll-back, which is a common event associated with slab tears, caused hot asthenospheric (undepleted mantle) to flow into a tear in the

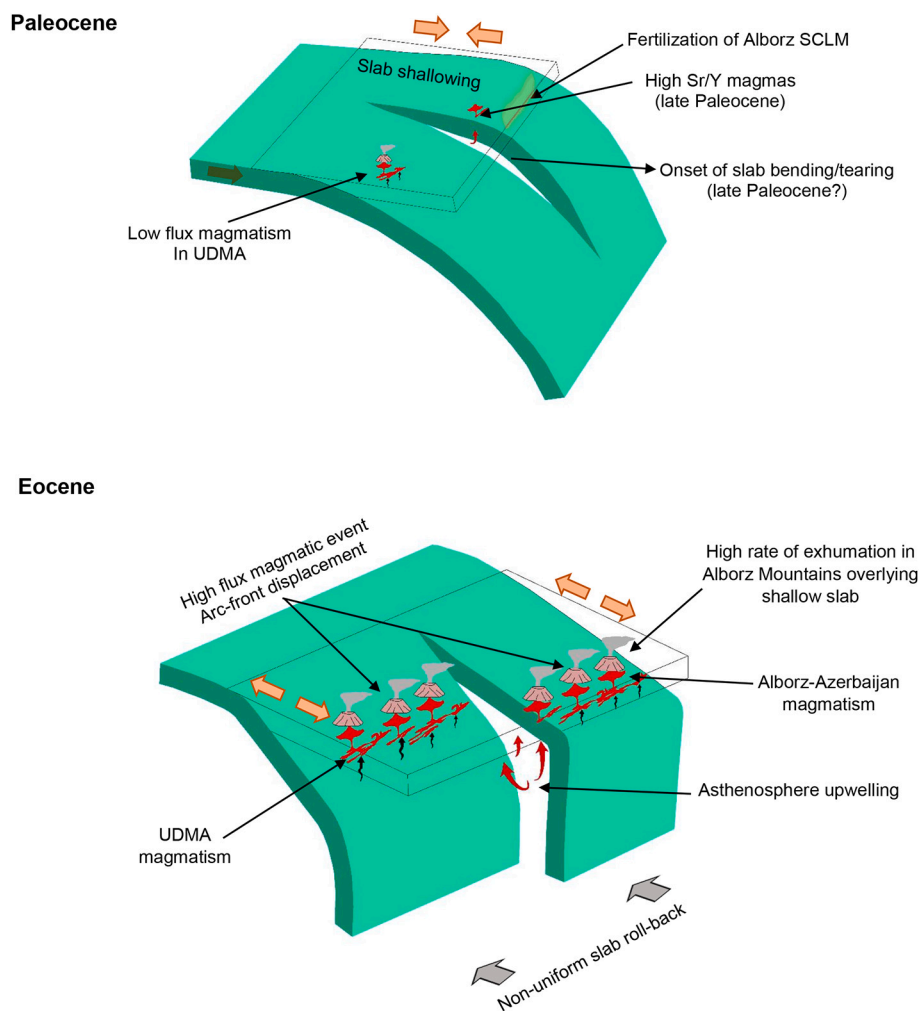


Fig. 18. Schematic cartoon (not to scale) illustrating the proposed geodynamic scenario for the evolution of Neotethyan subduction during Paleocene to Eocene time interval. (a) The subduction of positively buoyant feature (such as aseismic ridges/oceanic plateau/intraplate island/seamount chains) in the northern part of the Neotethyan subduction system led to the development of shallow dipping slab beneath the Alborz- Azerbaijan zone. The transition from shallow slab to steep slab is likely achieved through gradual slab bending/tearing. This process is associated with low-flux magmatism in the UDMA (e.g., Agard et al., 2011) and compressional regime in the Alborz Mountains (e.g., Guest et al., 2006) during the Paleocene. Modification/fertilization of SCLM underlying the Alborz-Azarbayjan zone is amplified by shallow slab components (b) Development of slab tearing associated with non-uniform slab roll-back and asthenosphere upwelling caused regional extension, high voluminous magmatism and arc-front displacement.

subducting slab and triggered partial melting of SCLM beneath the Alborz and UDMA. The slight geochemical transition of Alborz magmas towards enriched asthenospheric mantle-derived melts (e.g., Figs. 13;14b, c; 15f; 16d; 17a, b) compared to the UDMA might have resulted from differences in the SCLM underlying Alborz mountains, which had been less affected by the Neotethyan subduction and acted as a more fertile mantle compared to the SCLM underneath UDMA. Furthermore, the SCLM heterogeneity associated with a variable degree and depth of partial melting in the UDMA, as well as differentiation and contamination of the primary magmas within the relatively thick active continental margin, led to a larger range of melt compositions along the UDMA compared to the Alborz. The non-uniform slab roll-back associated with asthenospheric upwelling might be a plausible mechanism to influence most parts of the Iranian plate (as overriding plate) and trigger lithospheric thinning and partial melting of SCLM.

7. Conclusion

Eocene high-K calc-alkaline to alkaline shoshonitic volcanic rocks from the Alborz Mountains show geochemical signatures characteristic of a subduction environment. Comparisons between the Eocene magmas

in the Alborz and UDMA suggest many geochemical similarities, but we found lower degrees of partial melting, as well as a contribution of deeper mantle material in the genesis of the Alborz magmas than in the UDMA. The lower degrees of partial melting in the Alborz are best explained by the addition of sediment-derived melts (lower amounts of fluids) to the lithospheric mantle. Miocene samples from the UDMA show intermediate to felsic compositions with geochemical and zircon Hf isotopic data that point to the partial melting of mafic to intermediate lower crust triggered by juvenile mantle derived melts. Thermochronological data suggest rapid cooling through crystallization temperatures in the middle to late Eocene and the late Oligocene to early Miocene exhumation phase due to the unroofing of intrusive bodies through shallow crustal depths. Among various geodynamic scenarios presented for the evolution of the Eocene magmatic flare-up along the UDMA and the Alborz magmatic belts, a change in geometry of the subducting slab associated with slab bending/tearing and non-uniform slab roll-back is best supported by our data. Subsequent asthenosphere upwelling through the slab tear influenced the arc magmatism in the Alborz Mountains.

Supplementary data to this article can be found online at <https://doi.org/10.1016/j.chemgeo.2023.121889>.

CRedit authorship contribution statement

Maryam Honarmand: Conceptualization, Formal analysis, Interpretation, Writing – original draft, Writing - Review & Editing. **Annique van der Boon:** Investigation, Formal analysis, Writing - Review & Editing. **Franz Neubauer:** Investigation, Formal analysis. **Bianca Heberer:** Investigation, Formal analysis, Writing - Review & Editing. **Qiuli Li:** Investigation, Formal analysis. **Klaudia F. Kuiper:** Investigation, Formal analysis, Writing - Review & Editing. **Paul R.D. Mason:** Investigation, Formal analysis, Writing - Review & Editing. **Wout Krijgsman:** Investigation, Funding acquisition.

Declaration of Competing Interest

The authors declare the following financial interests/personal relationships which may be considered as potential competing interests:

Maryam Honarmand reports was provided by Institute for Advanced Studies in Basic Sciences. Maryam Honarmand reports a relationship with Institute for Advanced Studies in Basic Sciences that includes: employment.

Data availability

Data will be made available on request.

Acknowledgments

This work benefited greatly from projects provided in Iran, Europe and China. The whole rock geochemical data and part of the Ar/Ar data were supported by Utrecht University and the Vrije Universiteit Amsterdam, respectively. The zircon U-Pb and Lu-Hf isotopic data were provided by Chinese Academy of Sciences (National Key R and D Program of China; 2016YFE0203000). Part of Ar/Ar and thermochronology data were obtained from the Salzburg University. The logistical support for field studies came from Utrecht University and Institute for Advanced Studies in Basic Sciences (IASBS), Zanjan, Iran. AvdB. acknowledges financial support from the Research Council of Norway through its Centres of Excellence scheme, project number 332523 (PHAB), as well as project number 334622 (Young Talent scheme, project PANDA). We thank editor Balz Kamber, Guido Gianni and anonymous reviewers for their comments that have improved this paper.

References

- Agard, P., Omrani, J., Jolivet, L., Whitechurch, H., Vrielynck, B., Spakman, W., Monie, P., Meyer, B., Wortel, R., 2011. Zagros orogeny: a subduction-dominated process. *Geol. Mag.* 148, 692–725.
- Aghazadeh, M., Castro, A., Badrzadeh, Z., Vogt, K., 2011. Post-collisional polycyclic plutonism from the Zagros hinterland: the Shaivar Dagh plutonic complex, Alborz belt, Iran. *Geol. Mag.* 148, 980–1008.
- Aldanmaz, E., Pearce, J.A., Thirlwall, M., Mitchell, J., 2000. Petrogenetic evolution of late Cenozoic, post-collision volcanism in western Anatolia, Turkey. *J. Volcanol. Geotherm. Res.* 102, 67–95.
- Alirezadeh, A., Arvin, M., Dargahi, S., 2017. Adakite-like signature of porphyry granitoid stocks in the Meiduk and Parkam porphyry copper deposits, NE of Shahr-e-Babak, Kerman, Iran: constrains on geochemistry. *Ore Geol. Rev.* 88, 370–383.
- Allen, M.B., Ghassemi, M.R., Shahrabi, M., Qorashi, M., 2003. Accommodation of late Cenozoic oblique shortening in the Alborz range, northern Iran. *J. Struct. Geol.* 25, 659–672. [https://doi.org/10.1016/S0191-8141\(02\)00064-0](https://doi.org/10.1016/S0191-8141(02)00064-0).
- Amidi, S.M., 1984. Geological map of the Saveh, Scale 1:250,000. Geological Survey of Iran.
- Asiabanha, A., Foden, J., 2012. Post-collisional transition from an extensional volcano-sedimentary basin to a continental arc in the Alborz Ranges, N-Iran. *Lithos* 148, 98–111.
- Asiabanha, A., Ghasemi, H., Meshkin, M., 2009. Paleogene continental-arc type volcanism in North Qazvin, North Iran: facies analysis and geochemistry. *Neues Jahrb. Mineral. Abhandl.* 186, 201–214.
- Axen, G.J., Lam, P.J., Grove, M., Stockli, D.F., Hassanzadeh, J., 2001. Exhumation of the west-central Alborz Mountains, Iran, Caspian subsidence, and collision related tectonics. *Geology* 29, 559–562.
- Azizi, H., Jahangiri, A., 2008. Cretaceous subduction-related volcanism in the northern Sanandaj-Sirjan Zone, Iran. *J. Geodyn.* 45, 178–190.
- Azizi, H., Tsuboi, M., 2021. The van microplate: a new microcontinent at the Junction of Iran, Turkey, and Armenia. *Front. Earth Sci.* 8, 574385 <https://doi.org/10.3389/feart.2020.574385>.
- Babazadeh, S., D'Antonio, M., Cottle, J.M., Ghalamghash, J., Raeisi, D., An, Y., 2021. Constraints from geochemistry, zircon U-Pb geochronology and Hf-Nd isotopic compositions on the origin of Cenozoic volcanic rocks from central Urmia-Dokhtar magmatic arc, Iran. *Gondwana Res.* 90, 27–46.
- Ballato, P., Stockli, D.F., Ghassemi, M.R., Landgraf, A., Strecker, M.R., Hassanzadeh, J., Friedrich, A., Tabatabaei, S.H., 2013. Accommodation of transpressional strain in the Arabia-Eurasia collision zone: new constraints from (U-Th)/He thermochronology in the Alborz Mountains, North Iran. *Tectonics* 32, 1–18.
- Beccaluva, L., Bianchini, G., Bonadiman, C., Siena, F., Vaccaro, C., 2004. Coexisting anorogenic and subduction-related metasomatism in the mantle xenoliths from the Betic Cordillera (southern Spain). *Lithos* 75, 67–87.
- Berberian, M., King, G.C.P., 1981. Towards a paleogeography and tectonic evolution of Iran. *Can. J. Earth Sci.* 18, 210–265. <https://doi.org/10.1139/e81-163>.
- Blichert-Toft, J., Albareda, F., 1997. The Lu-Hf isotope geochemistry of chondrites and the evolution of the mantle-crust system. *Earth Planet. Sci. Lett.* 148, 243–258.
- Boehnke, P., Watson, E.B., Trail, D., Harrison, T.M., Schmitt, A.K., 2013. Zircon saturation re-revisited. *Chem. Geol.* 351, 324–334. <https://doi.org/10.1016/j.chemgeo.2013.05.028>.
- Boonma, K., García-Castellanos, D., Jiménez-Munt, I., Gerya, T., 2023. Thermomechanical modelling of lithospheric slab tearing and its topographic response. *Front. Earth Sci.* 11, 1095229. <https://doi.org/10.3389/feart.2023.1095229>.
- Cao, W., Paterson, S., Memeti, V., Mundil, R., Anderson, J.L., Schmidt, K., 2015. Tracking paleodeformation fields in the Mesozoic Central Sierra Nevada arc: implications for intra-arc cyclic deformation and arc tempos. *Lithosphere* 7, 296–320. <https://doi.org/10.1130/L389.1>.
- Castellanos, J.C., Clayton, R.W., Pérez-Campos, X., 2018. Imaging the eastern Trans-Mexican Volcanic Belt with ambient seismic noise: evidence for a slab tear. *J. Geophys. Res. Solid Earth* 123, 7741–7759. <https://doi.org/10.1029/2018JB015783>.
- Castro, A., Aghazadeh, M., Badrzadeh, Z., Chichorro, M., 2013. Late Eocene-Oligocene post-collisional monzonitic intrusions from the Alborz magmatic belt, NW Iran. An example of monzonite magma generation from a metasomatized mantle source. *Lithos* 180, 109–127.
- Chen, L., Jiang, M., Talebian, M., Ghods, A., Chung, S.L., Ai, Y., Sobouti, F., He, Y., Motaghi, Kh., Zheng, T., Faridi, M., Chen, Q.F., Lyu, Y., Xiao, W., Jafari, M., Zhu, R., 2016. New seismic array observation in the Northwestern Iranian Plateau. *Geophys. Res. Abstr.* 18, EGU 2016-3427.
- Chiu, H.Y., Chung, S.L., Zarrinkoub, M.H., Mohammadi, S.S., Khatib, M.M., Iizuka, Y., 2013. Zircon U-Pb age constraints from Iran on the magmatic evolution related to Neotethyan subduction and Zagros orogeny. *Lithos* 162, 70–87.
- Chiu, H.Y., Chung, S.L., Zarrinkoub, M.H., Melkonyan, R., Pang, K.N., Lee, H.Y., Wang, K.L., Mohammadi, S.S., Khatib, M.M., 2017. Zircon Hf isotopic constraints on magmatic and tectonic evolution in Iran: implications for crustal growth in the Tethyan orogenic belt. *J. Asian Earth Sci.* 145, 652–669.
- Cloos, M., 1993. Lithospheric buoyancy and collisional orogenesis: subduction of oceanic plateaus, continental margins, island arcs, spreading ridges, and seamounts. *Geol. Soc. Am. Bull.* 105, 715–737.
- Cocchi, L., Passaro, S., Tontini, F.C., Ventura, G., 2017. Volcanism in slab tear faults is larger than in island-arcs and back-arcs. *Nat. Commun.* 8 (1), 1–12.
- Conceição, R., Green, D., 2004. Derivation of potassic (shoshonitic) magmas by decompression melting of phlogopite + pargasite lherzolite. *Lithos* 72, 209–229.
- Condie, K.C., 2005. TTGs and adakites: are they both slab melts? *Lithos* 80, 33–44.
- Coticelli, S., Guarnieri, L., Farinelli, A., Mattei, M., Avanzinelli, R., Bianchini, G., Boari, E., Tommasini, S., Tiepolo, M., Prelevic, D., Venturiello, G., 2009. Trace elements and Sr–Nd–Pb isotopes of K-rich, shoshonitic, and calc-alkaline magmatism of the Western Mediterranean Region: genesis of ultrapotassic to calc-alkaline magmatic associations in a post-collisional geodynamic setting. *Lithos* 107, 68–92.
- Couzinie, S., Laurent, O., Moyen, J.-F., Zeh, A., Bouilhol, P., Villaras, A., 2016. Post-collisional magmatism: crustal growth not identified by zircon Hf-O isotopes. *Earth Planet. Sci. Lett.* 456, 182–195.
- Davaille, A., Lees, J.M., 2004. Thermal modeling of subducted plates: tear and hotspot at the Kamchatka corner. *Earth Planet. Sci. Lett.* 226, 293–304.
- Davies, R., Jones, C.R., Hamzepour, B., Clark, G.C., 1972. *Geology of Masuleh Sheet, D3*. Geological Survey of Iran, Tehran, p. 198.
- De Silva, S.L., Kay, S.M., 2018. Turning up the heat: high-flux magmatism in the Central Andes. *Elements* 14, 245–250. <https://doi.org/10.2138/gselements.14.4.245>.
- Deevsalar, R., Shinjo, R., Ghaderi, M., Murata, M., Hoskin, P.W.O., Oshiro, S., Wang, K.-L., Lee, H.Y., Neill, I., 2017. Mesozoic-Cenozoic mafic magmatism in Sanandaj-Sirjan Zone, Zagros Orogen (Western Iran): geochemical and isotopic inferences from Middle Jurassic and Late Eocene gabbros. *Lithos* 284–85, 588–607. <https://doi.org/10.1016/j.lithos.2017.05.009>.
- Dimalanta, C.B., Yumul, J.G.P., 2008. Crustal thickness and adakite occurrence in the Philippines: is there a relationship? *Island Arc* 17, 421–431.
- Doroozi, R., Vaccaro, C., Masoudi, F., Petrini, R., 2016. Cretaceous alkaline volcanism in south Marzanabad, northern central Alborz, Iran: geochemistry and petrogenesis. *Geosci. Front.* 7, 937–951.
- Ducea, M.N., Barton, M.D., 2007. Igniting flare-up events in Cordilleran arcs. *Geology* 35, 1047–1050. <https://doi.org/10.1130/G23898A.1>.

- Ebrahimi, L., Tabatabaei Manesh, M., 2016. Petrography and geochemistry of volcanic rocks in the east of Nabar (SW of Kashan) with emphasis on the role of crustal contamination. *Petrology* 7, 83–104.
- Eftekhari-nejad, J., 1987. Geological map of the Ardabil, Scale 1:250,000. Geological Survey of Iran.
- Esna-Ashari, A., Tiepolo, M., Valizadeh, M.V., Hassanzadeh, J., Sepahi, A.A., 2012. Geochemistry and zircon U-Pb geochronology of Aligoodarz granitoid complex, Sanandaj-Sirjan Zone, Iran. *J. Asian Earth Sci.* 43, 11–22.
- Etemad-Saeed, N., Hosseini-Barzi, M., Adabi, M., Miller, N.R., Sadeghi, A., Houshmandzadeh, A., Stockli, D.F., 2016. Evidence for ca. 560 Ma Ediacaran glaciation in the Kahar Formation, central Alborz Mountains, northern Iran. *Gondwana Res.* 31, 164–183.
- Ferrari, L., 2004. Slab detachment control on mafic volcanic pulse and mantle heterogeneity in Central Mexico. *Geology* 32, 77–80.
- Fitzgerald, P.G., Fryxell, J.E., Wernicke, B.P., 1991. Miocene crustal extension and uplift in southeastern Nevada — constraints from fission-track analysis. *Geology* 19, 1013–1016.
- Förster, H., Fesefeldt, K., Kürsten, M., 1972. Magmatic and orogenic evolution of the central Iranian volcanic belt. In: Armstrong, J.E., Hedberg, H.D. (Eds.), 24th International Geologic Congress. Montreal, QC, Canada, International Geology Congress, pp. 198–210.
- François, T., Agard, P., Bernet, M., Meyer, B., Chung, S.-L., Zarrinkoub, M.H., Burov, E., Monié, P., 2014. Cenozoic exhumation of the internal Zagros: first constraints from low-temperature thermochronology and implications for the build-up of the Iranian plateau. *Lithos* 206–207, 100–112.
- Furman, T., Graham, D., 1999. Erosion of lithospheric mantle beneath the East African Rift system: geochemical evidence from the Kivu volcanic province. *Lithos* 48, 237–262.
- Gale, A., Dalton, C.A., Langmuir, C.H., Su, Y., Schilling, J.-G., 2013. The mean composition of ocean ridge basalts. *Geochem. Geophys. Geosyst.* 14, 489–518.
- Georgieva, V., Gallagher, K., Sobczyk, A., Sobel, E.R., Schildgen, T.F., Ehlers, T.A., Strecker, M.R., 2019. Effects of slab-window, alkaline volcanism, and glaciation on the thermochronometer cooling histories, Patagonian Andes. *Earth Planet. Sci. Lett.* 511, 164–176.
- Gérault, M., Husson, L., Miller, M.S., Humphreys, E.D., 2015. Flat-slab subduction, topography, and mantle dynamics in southwest-ern Mexico. *Tectonics* 34, 1892–1909. <https://doi.org/10.1002/2015TC003908>.
- Ghasemi, A., Talbot, C.J., 2006. A new scenario for the Sanandaj-Sirjan zone (Iran). *J. Asian Earth Sci.* 26, 683–693.
- Ghorbani, M.R., Bezenjani, R.N., 2011. Slab partial melts from the metasomatizing agent to adakite, Tafresh Eocene volcanic rocks, Iran. *Island Arc* 20, 188–202.
- Gianni, G.M., Navarrete, C., Spagnotto, S., 2019. Surface and mantle records reveal an ancient slab tear beneath Gondwana. *Scientific Reports. Nature.* <https://doi.org/10.1038/s41598-019-56335-9>.
- Govers, R., Wortel, M.J.R., 2005. Lithosphere tearing at STEP faults: response to edges of subduction zones. *Earth Planet. Sci. Lett.* 236, 505–523.
- Guest, B., Stockli, D.F., Grove, M., Axen, G.J., Lam, P.S., Hassanzadeh, J., 2006. Thermal histories from the central Alborz Mountains, northern Iran: implications for the spatial and temporal distribution of deformation in northern Iran. *Geol. Soc. Am. Bull.* 118 (11/12), 1507–1521.
- Guillot, M.G., Escayola, M., Acevedo, R., 2011. Calc-alkaline rear-arc magmatism in the Fuegian Andes: implications for the mid-cretaceous tectonomagmatic evolution of southernmost South America. *J. S. Am. Earth Sci.* 31, 1–16.
- Hafkenscheid, E., Wortel, M.J.R., Spakman, W., 2006. Subduction history of the Tethyan region derived from seismic tomography and tectonic reconstructions. *J. Geophys. Res.* 111, B08401. <https://doi.org/10.1029/2005JB003791>.
- Harrison, T.M., Duncan, I., McDougall, I., 1985. Diffusion of ⁴⁰Ar in biotite — temperature, pressure and compositional effects. *Geochim. Cosmochim. Acta* 49, 2461–2468.
- Hassanzadeh, J., 1993. Metallogenic and Tectono-Magmatic Events in the SE Sector of the Cenozoic Active Continental Margin of Central Iran (Shahr e Babak Area, Kerman Province). Ph.D. thesis, 204 pp. Univ. of Calif, Los Angeles.
- Hassanzadeh, J., Wernicke, B.P., 2016. The Neotethyan Sanandaj-Sirjan zone of Iran as an archetype for passive margin-arc transitions. *Tectonics* 35, 586–621.
- Hassanzadeh, J., Stockli, D.F., Horton, B.K., Axen, G.J., Stockli, L.D., Grove, M., Schmitt, A.K., Walker, J.D., 2008. U – Pb zircon geochronology of late Neoproterozoic – early Cambrian granitoids in Iran: implications for paleogeography, magmatism, and exhumation history of Iranian basement. *Tectonophysics* 451, 71–96.
- Honarmand, M., Omran, N.R., Corfu, F., Emami, M.H., Nabatian, G., 2013. Geochronology and magmatic history of a calc-alkaline plutonic complex in the Urmia-Dokhtar Magmatic Belt, Central Iran: zircon ages as evidence for two major plutonic episodes. *Neues Jahrb. Mineral. Abhandl.* 190, 67–77.
- Honarmand, M., Omran, N.R., Neubauer, F., Emami, M. H., Nabatian, G., Liu, X. M., Dong, Y. P., von Quadt, A., Chen, B., 2014. Laser-ICP-MS U-Pb zircon ages and geochemical and Sr-Nd-Pb isotopic compositions of the Niyasar plutonic complex, Iran: constraints on petrogenesis and tectonic evolution. *Int. Geol. Rev.*, v. 56, p. 104–132.
- Honarmand, M., Li, X.H., Nabatian, Gh., Rezaei, M., Etemad-Saeed, N., 2016. Neoproterozoic-early Cambrian tectono-magmatic evolution of the central Iranian terrane, northern margin of Gondwana: constraints from detrital zircon U-Pb and Hf-O isotope studies. *Gondwana Res.* <https://doi.org/10.1016/j.gr.2016.05.007>.
- Honarmand, M., Xiao, W., Nabatian, Gh., Blades, M.L., Santos, M.C., Collins, A.S., Ao, S., 2018. Zircon U-Pb-Hf isotopes, bulk-rock geochemistry and Sr-Nd-Pb isotopes from late Neoproterozoic basement in the Mahneshan area, NW Iran: implications for Ediacaran active continental margin along the northern Gondwana and constraints on the late Oligocene crustal anatexis. *Gondwana Res.* 57, 48–76.
- Hossein Shomali, Z., Keshvari, F., Hassanzadeh, J., Mirzaei, N., 2011. Lithospheric structure beneath the Zagros collision zone resolved by non-linear teleseismic tomography. *Geophys. J. Int.* 187, 394–406.
- House, M.A., Farley, K.A., Kohn, B.P., 1999. An empirical test of helium diffusion in apatite: borehole data from the Otway basin, Australia. *Earth Planet. Sci. Lett.* 170, 463–474.
- Hu, J., Liu, L., 2016. Abnormal seismological and magmatic processes controlled by the tearing South American flat slabs. *Earth Planet. Sci. Lett.* 450, 40–51.
- Ishikawa, T., Nakamura, E., 1994. Origin of the slab component in arc lavas from across-arc variation of B and Pb isotopes. *Nature* 370, 205–208.
- Jahangiri, A., 2007. Post-collisional Miocene adakitic volcanism in NW Iran: geochemical and geodynamic implications. *J. Asian Earth Sci.* 30, 433–447.
- Jolivet, M., Menant, A., Sternai, P., Rabillard, A., Arbaret, L., Augier, R., Laurent, V., Beaudoin, A., Grasmann, B., Huet, B., Labrousse, L., Le Pourhiet, L., 2015. The geological signature of a slab tear below the Aegean. *Tectonophysics* 659, 166–182.
- Jung, C., Jung, S., Hoffer, E., Berndt, J., 2006. Petrogenesis of Tertiary mafic alkaline magmas in the Hoheifel, Germany. *J. Petrol.* 47, 1637–1671.
- Karimpour, M.H., Rezaei, M., Zarasvandi, A., Malekzadeh Shafaroudi, A., 2021. Saveh-Nain-Jiroft Magmatic Belt replaces Urmia-Dokhtar Magmatic Belt: investigation of genetic relationship between porphyry copper deposits and adakitic and non-adakitic granitoids. *J. Econ. Geol.* 13, 465–506.
- Kazemi, K., Kananian, Al, Xiao, P., Sarjoughian, F., 2019. Petrogenesis of Middle-Eocene granitoids and their Mafic microgranular enclaves in central Urmia-Dokhtar Magmatic Arc (Iran): evidence for interaction between felsic and mafic magmas. *Geosci. Front.* 10, 705–723.
- Keskin, M., 2003. Magma generation by slab steepening and breakoff beneath a subduction-accretion complex: An alternative model for collision-related volcanism in Eastern Anatolia, Turkey. *Geophys. Res. Lett.* 30, 8046. <https://doi.org/10.1029/2003GL018019>, 4 pp.
- Kheirkhah, M., Allen, M.B., Emami, M., 2009. Quaternary syncollisional magmatism from the Iran/Turkey borderlands. *J. Volcanol. Geotherm. Res.* 182, 1–12.
- Kiraly, A., Portner, D.E., Haynie, K.L., Chilson-Parks, B.H., Ghosh, T., Jadamec, M., Makushkina, A., Manga, M., Moresi, L., O'Farrel, K.A., 2020. The effect of slab gaps on subduction dynamics and mantle upwelling. *Tectonophysics*. 785, 228458 <https://doi.org/10.1016/j.tecto.2020.228458>.
- Kirchenbaur, M., Munker, C., Schuth, S., Garbe-Schonberg, D., Marchev, P., 2011. Tectonomagmatic constraints on the sources of Eastern Mediterranean K-rich Lavas. *J. Petrol.* 10, 1–39.
- Kuritani, T., Nakagawa, M., 2016. Origin of ultra-rear-arc magmatism at Rishiri Volcano, Kuril Arc. *Geochem. Geophys. Geosyst.* 17, 4032–4050. <https://doi.org/10.1002/2016GC006594>.
- Kuritani, T., Yokoyama, T., Nakamura, E., 2008. Generation of Rear-arc Magmas Induced by Influx of Slab-derived Supercritical Liquids: implications from Alkali Basalt Lavas from Rishiri Volcano, Kurile Arc. *J. Petrol.* 49, 1319–1342.
- Lasemi, Y. 1992. Submarine fans and turbidite deposits in the Karaj Formatin (Abstract). 10th Geoscience Meeting of the Geological Survey of Iran, p. 5.
- Le Bas, M.J., Lemaître, R.W., Streckeis, A., Zanettin, B., 1986. A chemical classification of volcanic-rocks based on the total alkali silica *Diagram*. *J. Petrol.* 27, No.3. <https://doi.org/10.1093/ptology/27.3.745>.
- Liu, X., Pysklywec, R., 2023. Transient injection of flow: how torn and bent slabs induce unusual mantle circulation patterns near a flat slab. *Geochem. Geophys. Geosyst.* 24 <https://doi.org/10.1029/2023GC011056> e2023GC011056.
- Lotfi, M., 2001. Geological Map of the Mahneshan, Scale 1:100,000 (Geological Survey of Iran).
- Lovera, O.M., Richter, F.M., Harrison, T.M., 1989. The ⁴⁰Ar/³⁹Ar thermochronometry for slowly cooled samples having a distribution of diffusion domain sizes. *J. Geophys. Res.* 94, 17917–17935.
- Maghdour-Mashhour, R., Hayes, B., Pang, K.N., Bolhar, R., Tabbakh Shabani, A.A., Elahi-Janatmak, F., 2021. Episodic subduction initiation triggered Jurassic magmatism in the Sanandaj-Sirjan zone, Iran. *Lithos* 396–397.
- Mahmoudi, S., Corfu, F., Masoudi, F., Mehrabi, B., Mohajjel, M., 2011. U-Pb dating and emplacement history of granitoid plutons in the northern Sanandaj-Sirjan Zone, Iran. *J. Asian Earth Sci.* 41, 238–249.
- Masson, F.D.R., Anvari, M., Djamour, Y., Walpersdorf, A., Tavakoli, F., Daignières, M., Nankali, H., Van Gorp, S.B., 2007. Large-scale velocity field and strain tensor in Iran inferred from GPS measurements: new insight for the present-day deformation pattern within NE Iran. *Geophys. J. Int.* 170, 436–440.
- Mayer, B., Jung, S., Romer, R.L., Stracke, A., Haase, K.M., Garbe-Schonberg, C.D., 2013. Petrogenesis of Tertiary Hornblende-bearing Lavas in the Rhon, Germany. *J. Petrol.* 54, 2095–2123.
- McKenzie, D., O'Nions, R.K., 1991. Partial melt distributions from inversion of rare earth element concentrations. *J. Petrol.* 32, 1021–1091.
- McQuarrie, N., van Hinsbergen, D.J.J., 2013. Retrodeforming the Arabia-Eurasia collision zone: age of collision versus magnitude of continental subduction. *Geology* 41, 315–318.
- Miyazaki, T., Gill, J.B., Hamelin, C., DeBari, S.M., Sato, T., Tamura, Y., et al., 2020. The first 10 million years of rear-arc magmas following backarc basin formation behind the Izu arc. *Geochem. Geophys. Geosyst.* 21 <https://doi.org/10.1029/2020GC009114> e2020GC009114.
- Moghadam, H., Griffin, W.L., Li, X.H., Santos, J.F., Karsli, O., Stern, R.J., Ghorbani, G., Gain, S., Murphy, R., O'Reilly, S.Y., 2018. Crustal evolution of NW Iran: Cadomian Arcs, Archean fragments and the cenozoic magmatic Flare-up. *J. Petrol.* 58, 2143–2190.
- Moghadam, H.S., Li, Q.L., Li, X.H., Stern, R.J., Levresse, G., Santos, J.F., Martinez, M.L., Ducea, M.N., Ghorbani, G., Hassannezhad, A., 2020. Neotethyan subduction ignited

- the Iran Arc and backarc differently. *J. Geophys. Res. Solid Earth* 125. <https://doi.org/10.1029/2019JB018460> e2019JB018460.
- Mohajjel, M., Fergusson, C.L., Sahandi, M.R., 2003. Cretaceous-Tertiary convergence and continental collision, Sanandaj-Sirjan Zone, western Iran. *J. Asian Earth Sci.* 21, 397–412.
- Mokhtari, M.A., Kouhestani, H., Pang, K.N., Hsu, S.C., Chung, S.L., Lee, H.Y., 2021. Early Eocene high-Sr/Y magmas from the Urmia-Dokhtar paleo-arc, Iran: implications for the origin of high-flux events in magmatic arcs. *Lithos* 416–417, 106656. <https://doi.org/10.1016/j.lithos.2022.106656>.
- Morley, C.K., Kongwung, B., Julapour, A.A., Abdolghafourian, M., Hajian, M., Waples, D., Warren, J., Otterdoorn, H., Srisuriyon, K., Kazemi, H., 2009. Structural development of a major late Cenozoic basin and transpressional belt in Central Iran: the Central Basin in the Qom-Saveh area. *Geosphere* 5 (4), 325–362.
- Motaghi, K., Shabaniyan, E., Tatar, M., Cuffaro, M., Doglioni, C., 2017. The south Zagros suture zone in teleseismic images. *Tectonophysics* 694, 292–301.
- Motaghi, K., Shabaniyan, E., Nozad-Khalil, T., 2020. Deep structure of the western coast of the Makran subduction zone, SE Iran. *Tectonophysics* 776, 228314.
- Mouthereau, F., Lacombe, O., Verges, J., 2012. Building the Zagros collisional orogen: timing, strain distribution and the dynamics of Arabia/Eurasia plate convergence. *Tectonophysics* 532, 27–60.
- Murphy, J.B., 2016. The role of the ancestral Yellowstone plume in the tectonic evolution of the western United States. *Geosci. Can.* 43, 231–250.
- Nabatian, G., Ghaderi, M., Neubauer, F., Honarmand, M., Liu, X., Dong, M., Jiang, S.Y., von Quadt, A., Bernroider, M., 2014. Petrogenesis of Tarom high-potassic granitoids in the Alborz-Azarbaijan belt, Iran: geochemical, U-Pb zircon and Sr-Nd-Pb isotopic constraints. *Lithos* 184, 324–345.
- Nabatian, G., Jiang, S.Y., Honarmand, M., Neubauer, F., 2016a. Zircon U-Pb ages, geochemical and Sr-Nd-Pb-Hf isotopic constraints on petrogenesis of the Tarom-Olya pluton, Alborz magmatic belt, NW Iran. *Lithos* 244, 43–58.
- Nabatian, G., Ghaderi, M., Honarmand, M., 2016b. Petrography and mineral chemistry of Tarom plutonic complex, NE Zanjan. *Petrology* 26, 99–116.
- Nabatian, G., Li, X.H., Honarmand, M., Melgarejo, J.C., 2017. Geology, mineralogy and evolution of iron skarn deposits in the Zanjan district, NW Iran: constraints from U-Pb dating, Hf and O isotope analyses of zircons and stable isotope geochemistry. *Ore Geol. Rev.* 84, 42–66.
- Omrani, J., Agard, P., Whitechurch, H., Benoit, M., Prouteau, G., Jolivet, L., 2008. Arc-magmatism and subduction history beneath the Zagros Mountains, Iran: a new report of adakites and geodynamic consequences. *Lithos* 106, 380–398.
- Paul, P., Hatzfeld, D., Kaviani, A., Tatar, M., Péquignat, C., 2010. Seismic imaging of the lithospheric structure of the Zagros mountain belt (Iran). *Geol. Soc. Lond. Spec. Publ.* 330, 5–18.
- Pearce, J.A., Parkinson, L.J., 1993. Trace element models for mantle melting: application to volcanic arc petrogenesis. *Geol. Soc. Lond. Spec. Publ.* 76, 373–403. <https://doi.org/10.1144/gsl.sp.1993.076.01.19>.
- Pearce, J.A. and Stern, R.J. 2006. Origin of back-arc basin magmas: trace element and isotope perspectives. In: Christie D.M., Fisher C.R., Lee S-M., Givens S. (eds) Back-arc spreading systems: geological, biological, chemical, and physical interactions. *Geophysical Monograph Series*, 166, *Advancing Earth and Space Sciences*, p. 63–86.
- Pe-Piper, G., Zhang, Y., Piper, D.J.W., Prelevi, C. D., 2014. Relationship of Mediterranean type lamproites to large shoshonite volcanoes, Miocene of Lesbos, NE Aegean Sea. *Lithos* 184–187, 281–299.
- Prelevic, D., Akal, C., Romer, R.L., Foley, S.F., 2010. Lamproites as indicators of accretion and/or shallow subduction in the assembly of South-Western Anatolia, Turkey. *Terra Nova* 22, 443–452.
- Prelevic, D., Akal, C., Romer, R.L., Mertz-Kraus, R., Helvacı, C., 2015. Magmatic response to slab tearing: constraints from the Afyon Alkaline Volcanic Complex, Western Turkey. *J. Petrol.* 1–36.
- Rabiee, A., Rossetti, F., Asahara, Y., Azizi, H., Lucci, F., Lustrino, M., Nozaem, R., 2020. Long-lived, Eocene-Miocene stationary magmatism in NW Iran along a transform plate boundary. *Gondwana Res.* <https://doi.org/10.1016/j.gr.2020.03.014>.
- Raeisi, D., Zhao, M., Babazadeh, S., Long, L.E., Hajsadeghi, S., Modabberi, S., 2021. Synthesis on productive, sub-productive and barren intrusions in the Urmia-Dokhtar magmatic arc, Iran, constraints on geochronology and geochemistry. *Ore Geol. Rev.* 132, 103997.
- Rahmani, M., Motaghi, K., Ghods, A., Sobouti, F., Talebian, M., Ai, Y., Chen, L., 2019. Deep velocity image of the north Zagros collision zone (Iran) from regional and teleseismic tomography. *Geophys. J. Int.* 219 (3), 1729–1740.
- Regard, V., Hatzfeld, D., Molinaro, M., Aubourg, C., Bayer, R., Bellier, O., Yamini-Fard, F., Peyret, M., Abbassi, M., 2010. The transition between Makran subduction and the Zagros collision: recent advances in its structure and active deformation. In: Leturmy, P., Robin, C. (Eds.), *Tectonic and Stratigraphic Evolution of Zagros and Makran during the Mesozoic–Cenozoic*. Geological Society of London, Special Publication, pp. 43–64 no. 330.
- Rezaeian, M., Carter, A., Hovius, N., Allen, M.B., 2012. Cenozoic exhumation history of the Alborz Mountains, Iran: new constraints from low-temperature chronometry. *Tectonics* 31. <https://doi.org/10.1029/2011TC002974>.
- Robinson, J.A.C., Wood, B.J., 1998. The depth of the spinel to garnet transition at the peridotite solidus. *Earth Planet. Sci. Lett.* 164, 277–284.
- Roche, V., Sternai, P., Guillou-Frottier, L., Menant, A., Jolivet, L., Bouchot, V., Gerya, T., 2018. Emplacement of metamorphic core complexes and associated geothermal systems controlled by slab dynamics. *Earth Planet. Sci. Lett.* 498, 322–333.
- Rollinson, H., 2008. Secular evolution of the continental crust: Implications for crust evolution models. *Geochim. Geophys. Geosyst.* 9, Q12010. <https://doi.org/10.1029/2008GC002262>.
- Rosenbaum, G., Lister, G.S., Duboz, C., 2002. Relative motions of Africa, Iberia and Europe during Alpine orogeny. *Tectonophysics* 359, 117–129.
- Roshan, H., Nasr Isfahani, A.K., 2015. Petrogenetic interpretation of Cu hosted Eocene volcanic rocks in southwest of Ardestan, East of Isfahan. *J. Biodivers. Environ. Sci.* 6 (2), 439–446.
- Royden, L.H., Husson, L., 2009. Subduction with variations in slab buoyancy: models and application to the Banda and Apennine systems. In: Lallemand, S.E., Fucciello, F. (Eds.), *Subduction Zone Geodynamics*. Springer, Berlin. https://doi.org/10.1007/978-3-540-87974-9_2, pp. 35–5.
- Rudnick, R.L., Gao, S., 2003. The composition of the continental crust. In: Rudnick, R.L. (Ed.), *The Crust*. Elsevier-Pergamon, Oxford, pp. 1–64.
- Rudnick, R.L., Gao, S., 2013. Composition of the continental crust. In: Rudnick, R.L. (Ed.), *Treatise on Geochemistry*, second edition. Elsevier, Oxford, pp. 1–51.
- Saginer, I., Gazel, E., Condie, C., Carr, M.J., 2013. Evolution of geochemical variations along the central American volcanic front. *Geochim. Geophys. Geosyst.* 14, 4504–4522.
- Sarjoughian, F., Javadi, S., Azizi, H., Ling, W., Asahara, Y., Lentz, D., 2019. Geochemical and Sr–Nd isotopic constraints on the genesis of the Soheyleh-PaKuh granitoid rocks (central Urmia-Dokhtar magmatic belt, Iran). *Int. Geol. Rev.* <https://doi.org/10.1080/00206814.2019.1579676>.
- Sarkarinejad, K., Azizi, A., 2008. Slip partitioning and inclined dextral transpression along the Zagros Thrust System, Iran. *J. Struct. Geol.* 30, 116–136.
- Schellart, W.P., 2010. Mount Etna–Iblean volcanism caused by rollback-induced upper mantle upwelling around the Ionian slab edge: an alternative to the plume model. *Geology* 38 (8), 691–694.
- Sepahi, A.A., Malvandi, F., 2008. Petrology of the Bouein Zahra-Naein plutonic complexes, Urmia-Dokhtar belt, Iran: with special reference to granitoids of the Saveh plutonic complex. *Neues Jahrb. Mineral. Abhandl.* 185, 99–115.
- Shahriari, Sh., Ghorbani, M.R., Nasiri Bezenjani, R., 2011. Geochemistry and petrology of NE Naragh volcanic rocks: island arc or active continental margin magmatism? *Iran. J. Crystallogr. Mineral.* 19 (2), 251–262.
- Shaw, D.M., 1970. Trace element fractionation during anatexis. *Geochim. Cosmochim. Acta* 34, 237–243.
- Smit, J., Burg, J.-P., Dolati, A., Sokoutis, D., 2010. Effects of mass waste events on thrust wedges: analogue experiments and application to the Makran accretionary wedge. *Tectonics* 29. <https://doi.org/10.1029/2009TC002526>. TC3003. 11 pp.
- Smith, E.I., Sánchez, A., Walker, J.D., Wang, K., 1999. Geochemistry of mafic magmas in the Hurricane Volcanic field, Utah: implications for small- and large-scale chemical variability of the lithospheric mantle. *J. Geol.* 107, 433–448.
- Sobolev, A.V., Hofmann, A.W., Kuzmin, D.V., Yaxley, G.M., Arndt, N.T., Chung, S.L., Danyshevsky, L.V., Elliott, T., Frey, F.A., Garcia, M.O., Gurenko, A.A., Kamenetsky, V.S., Kerr, A.C., Krivolutskaya, N.A., Matvienkov, V.V., Nikogosian, I. K., Rocholl, A., Sigurdsson, I.A., Sushchevskaya, N.M., Teklay, M., 2007. The amount of recycled crust in sources of mantle-derived melts. *Science* 316, 412–417.
- Söderlund, U., Patchett, P.J., Vervoort, J.D., Isachsen, C.E., 2004. The ^{176}Lu decay constant determined by Lu–Hf and U–Pb isotope systematics of Precambrian mafic intrusions. *Earth Planet. Sci. Lett.* 219, 311–324.
- Stampfli, G.M., 2000. Tethyan oceans. In: Bozkurt, E., Winchester, J.A., Piper, J.D. (Eds.), *Tectonics and Magmatism in Turkey and Surrounding Area*, Vol. 173. *Journal of Geological Society of London, Special Publications*, pp. 1–23.
- Stampfli, G.M., Borel, G.D., 2002. A plate tectonic model for the Paleozoic and Mesozoic constrained by dynamic plate boundaries and restored synthetic oceanic isochrons. *Earth Planet. Sci. Lett.* 196, 17–33.
- Stern, R.J., 2010. The anatomy and ontogeny of modern intra-oceanic arc systems. In: Kusky, T.M., Zhai, M.G., Xiao, W. (Eds.), *The Evolving Continents: Understanding Processes of Continental Growth*. Geological Society, Vol. 338. *Special Publications*, London, pp. 7–34.
- Stern, R.J., Shafaii Moghadam, H., Pirouz, M., Mooney, W., 2021. The geodynamic evolution of Iran. *Annu. Rev. Earth Planet. Sci.* 49, 9–36.
- Stöcklin, J., 1968. Structural history and tectonics of Iran: a review. *Am. Assoc. Pet. Geol. Bull.* 52, 1229–1258.
- Stöcklin, J., Eftekhari-nejad, J., 1969. Geological map of the Zanjan, Scale 1:250,000. Geological Survey of Iran.
- Straub, S.M., LaGatta, A.B., Pozzo, M.D., Lillian, A., Langmuir, C.H., 2008. Evidence from high-Ni olivines for a hybridized peridotite/pyroxenite source for orogenic andesites from the central Mexican Volcanic Belt. *Geochim. Geophys. Geosyst.* 9, Q03007.
- Sun, S.S., McDonough, W.F., 1989. Chemical and isotopic systematics of oceanic basalts: implications for mantle composition and processes. *Geol. Soc. Lond. Spec. Publ.* 42, 313–345.
- Taghipour, N., Mohammadi Laghay, H., 2014. Sara (Parkam) porphyry copper deposit in Kerman, Iran: petrography, geochemistry and geodynamic setting. *Geochim. J. v. 1*, No. 3.
- Taki, S., Darvishzadeh, A., Ghaderi, M., Khosrow, Tehrani, Kh., 2009. Lithologic sequence and geochemical characteristics of second phase of Paleogene volcanic rocks in Deylaman area, Western Alborz. *Iran. J. Crystallogr. Mineral.* 17 (2), 239–252 (in Persian).
- Tarverdzadeh, H., 2020. Gravity Modeling of Crustal Structure in NW Iran Using Computational Intelligence (Along a Profile Perpendicular to the Alborz and Zagros Mountain Ranges). Unpublished MSc Thesis. Institute for Advanced Studies in Basic Sciences, Department of Earth Sciences, Zanjan, Iran.
- Taylor, S.R., McLennan, S.M., 1996. The evolution of continental crust. *Sci. Am.* 274, 76–81.
- Taylor, S.R. and McLennan, S.M. 1985. *The Continental Crust: Its Composition and Evolution*. xvi 312 pp. Oxford, London, Edinburgh, Boston, Palo Alto, Melbourne: Blackwell Scientific. ISBN 0 632 01148 3. *Geological Magazine*. v.122, p. 673–674. doi:10.1017/S0016756800032167.

- Teknik, V., Ghods, A., Thybo, H., Artemieva, I.M., 2019. Crustal density structure of the northwestern Iranian Plateau. *Can. J. Earth Sci.* <https://doi.org/10.1139/cjes-2018-0232>.
- Thompson, R.N., Morrison, M.A., Hendry, G.L., Parry, S.J., 1984. An assessment of the relative roles of crust and mantle in magma genesis: an elemental approach. *Philos. Trans. R. Soc. Lond.* 549–590.
- Van der Boon, A., 2017. From Peri-Tethys to Paratethys: Basin Restriction and Anoxia in Central Eurasia Linked to Volcanic Belts in Iran. PhD dissertation, Utrecht University.
- Van der Boon, A., Kuiper, K., van der Ploeg, R., Cramwinckel, M., Honarmand, M., Sluijs, A., Krijgsman, W., 2021. Exploring a link between the Middle Eocene Climatic Optimum and Neotethys continental arc flare-up. *Clim. Past* 17, 229–239. <https://doi.org/10.5194/cp-2020-48>.
- Veisi, M., Sobouti, F., Chevrot, S., Abbasi, M., Shabanian, E., 2021. Upper mantle structure under the Zagros collision zone; insights from 3D teleseismic P-wave tomography. *Tectonophysics* 819, 229106. <https://doi.org/10.1016/j.tecto.2021.229106>.
- Verdel, C., Wernicke, B.P., Hassanzadeh, J., Guest, B., 2011. A Paleogene extensional arc flare -up in Iran. *Tectonics* 30. <https://doi.org/10.1029/2010TC002809>. TC3008.
- Vernant, P., Nilforoushan, F., Hatzfeld, D., Abbassi, M.R., Vigny, C., Masson, F., Nankali, H., Martinod, J., Ashtiani, A., Bayer, R., Tavakoli, F., Chery, J., 2004. Present-day crustal deformation and plate kinematics in the Middle East constrained by GPS measurements in Iran and northern Oman. *Geophys. J. Int.* 157, 381–398.
- Vervoort, J.D., Blichert-Toft, J., 1999. Evolution of the depleted mantle: Hf isotope evidence from juvenile rocks through time. *Geochim. Cosmochim. Acta* 63, 533–556.
- Vincent, S.J., Allen, M.B., Ismail-Zadeh, A.D., Flecker, R., Foland, K.A., Simmons, M.D., 2005. Insights from the Talysh of Azerbaijan into the Paleogene evolution of the South Caspian region. *Geol. Soc. Am. Bull.* 117, 1513–1533. <https://doi.org/10.1130/B25690.1>.
- Wang, X., Peng, P., Wang, C., Yang, S., 2016. Petrogenesis of the 2115 Ma Haicheng mafic sills from the Eastern North China Craton: implications for an intra-continental rifting. *Gondwana Res.* 39, 347–364.
- Woodhead, J., Eggins, S., Gamble, J., 1993. High field strength and transition element systematics in island arc and back-arc basin basalts: evidence for multi-phase melt extraction and a depleted mantle wedge. *Earth Planet. Sci. Lett.* 114 (4), 491–504.
- Yao, Z., Qin, Z., Mungall, K.J.E., 2018. Tectonic controls on Ni and Cu contents of primary mantle-derived magmas for the formation of magmatic sulfide deposits. *Am. Mineral.* 103, 1545–1567.
- Yassaghi, A., Naeimi, A., 2011. Structural analysis of the Gachsar sub-zone in central Alborz range; constrain for inversion tectonics followed by the range transverse faulting. *Int. J. Earth Sci.* 100 (6), 1237–1249. <https://doi.org/10.1007/s00531-010-0537-y>.
- Yeganehfar, H., Ghorbani, M.R., Shinjo, R., Ghaderi, M., 2013. Magmatic and geodynamic evolution of Urmia-Dokhtar basic volcanism, Central Iran: major, trace element, isotopic, and geochronologic implications. *Int. Geol. Rev.* 55, 767–786.
- Zanchi, A., Berra, F., Mattei, M., Ghassemi, M., Sabouri, J., 2006. Inversion tectonics in central Alborz, Iran. *J. Struct. Geol.* 28, 2023–2037. <https://doi.org/10.1016/j.jsg.2006.06.020>.
- Zanchi, A., Zanchetta, S., Berra, F., Mattei, M., Garzanti, E., Molyneux, S., Nawab, A., Sabouri, J., 2009. The Eo-Cimmerian (late? Triassic) orogeny in North Iran. In: Brunet, M.-F., Wilmsen, F., Granath, J.W. (Eds.), *South Caspian to Central Iran Basins*. Geological Society of London, London, UK, pp. 31–55 (Geological Society Special Publications, 312).
- Zeng, G., Huang, X.W., Zhou, M.F., Chen, L.H., Xu, X.S., 2016. Using chalcophile elements to constrain crustal contamination and xenolith-magma interaction in Cenozoic basalts of eastern China. *Lithos* 258–259, 163–172.
- Zindler, A., Hart, S.R., 1986. Chemical geodynamics. *Annu. Rev. Earth Planet. Sci.* 14, 493–571.